Internal Gravity Wave Emission into the Middle Atmosphere from a Model Tropospheric Jet

B. R. SUTHERLAND AND W. R. PELTIER

Department of Physics, University of Toronto, Toronto, Ontario, Canada

(Manuscript received 15 September 1994, in final form 23 January 1995)

ABSTRACT

A mechanism is investigated whereby large amplitude internal gravity waves (IGWs) may be excited by the tropospheric jet stream when this is driven to parallel shear instability following a rapid external forcing of the mean flow, a circumstance that might be realized, for example, through ageostrophic effects in the process of baroclinic wave development. A series of mean states are examined, first on the basis of linear theory, to determine the characteristics of the most unstable normal mode, which is expected to dominate the initial stages of flow evolution. Two-dimensional nonlinear numerical simulations of stratified, incompressible, Boussinesq flow in a periodic channel are also performed. On the basis of linear theory, the authors show that it is possible to assess whether IGWs will be strongly excited by examining whether the initial instability satisfies an easily calculable criterion that has been previously termed the "penetration condition." In cases in which the penetration condition is satisfied, large amplitude IGWs with the same horizontal phase speed and wavelength as the most unstable mode of linear theory are shown in the nonlinear simulations to radiate freely into the stratosphere, and the process of stabilization of the mean state is thereafter significantly influenced by the extraction and upward vertical transport of horizontal momentum by IGWs away from the mixing region. In cases in which the penetration condition is not satisfied, only very weak internal wave emission is observed. These small amplitude waves evidently develop through nonlinear mechanisms. On the basis of model calculations performed using initial conditions intended to simulate realizable midlatitude zonal flows, the authors demonstrate that the vertical flux of horizontal momentum delivered into the stratosphere by such shear instability could reach levels comparable to the fluxes associated with topographically forced internal waves that develop during severe downslope windstorm events. This raises the question as to whether there may be circumstances in which the action of gravity wave drag on the general circulation could be affected by the process of emission rather than by the process of absorption. The basis of all current IGW drag parameterization schemes employed in large-scale models is that momentum is being deposited into the mean flow by IGW breaking. The authors question the universal validity of this assumption.

1. Introduction

Since Hines (1960) showed that internal gravity waves (IGWs) generated at low levels may propagate vertically upward to ionospheric heights where the waves attain appreciable amplitudes, it has come to be believed that the momentum deposition associated with the "breaking" of IGWs in the middle and upper atmosphere constitutes a significant forcing of the mean flow. This was first pointed out by Hodges (1967, 1969) and has been further examined by Lindzen (1967, 1981) and others since. There currently exists a large body of indirect evidence demonstrating that internal gravity waves may be generated by both lower-tropospheric shear flows and by the tropospheric jet stream itself. For example, using an acoustic echo sounder, anemometers, and a microbarograph array, Hooke et al. (1973) have observed the generation of IGWs by instability of the planetary boundary layer. Herron and Tolstoy (1969), on the other hand, have shown that correlations exist between the proximity of the jet stream and fluctuating pressure signals observed on a ground-based array of microbarographs, and Keliher (1975) has proposed that these fluctuations may be linked to shear instability of tropospheric winds. Fritts and Nastrom (1992) have noted that lower-stratospheric turbulence, presumably induced by breaking waves, seems to be especially intense above both the midlatitude tropospheric jet stream and frontal systems. The observed intensity of turbulence in such regions is almost as extreme as that observed over mountainous terrain. Although the basic mechanism by which IGWs are generated through orographic forcing is well known [Peltier and Clark 1979; Peltier and Clark 1980; see also Gill (1982, section 6.8) for a general discussion] and although a better appreciation is being developed of the way in which IGWs may be excited in convectively active flows (Clark et al. 1986; Fovell et al. 1992), the generation of IGWs in unstable stratified shear flow, by comparison, is as yet poorly understood.

Corresponding author address: Dr. W. R. Peltier, Department of Physics, University of Toronto, Toronto, ON M5S 1A7, Canada.

Explanations for IGW excitation in stratified parallel flows based upon linear theory have been proposed by Lindzen (1974) and Lindzen and Rosenthal (1976), who examined the stability of a Kelvin–Helmholtz velocity profile with constant Brunt–Väisälä frequency (N); by Davis and Peltier (1976) and Lalas and Einaudi (1976), who examined the stability of a hyperbolic tangent shear flow in stratified fluid characterized either by constant or z-dependent N; and by Mastrantonio et al. (1976) who examined a flow more representative of the tropospheric jet stream. All of this analysis, including Davis and Peltier (1979), demonstrated that the presence of a rigid lower boundary contributes to the growth of two new branches of unstable normal modes in addition to the usual modes associated with Kelvin–Helmholtz (K–H) instability. In one of these new modal branches the instability couples directly with a propagating wave field in the upper levels of the model, while in the other branch the disturbance is evanescent. Invoking the idea of overreflection originally introduced by Jones (1968), Davis and Peltier (1976) and Lindzen and Rosenthal (1976) explained that these two classes of instability, consisting of resonant-propagating and resonant-trapped modes, may be seen to develop as a result of resonant overreflection and thus amplification of neutral waves propagating between a critical layer and the ground. This idea had also been explored earlier by Lindzen (1974) in the context of analysis based upon the step-discontinuous Kelvin–Helmholtz velocity profile. In all of these analyses, however, the growth rate of the radiating modes was found to be significantly smaller than the growth rate of the trapped K–H mode, suggesting that the spontaneous development of propagating disturbances in an unstable flow would be expected to be weak if not altogether prevented.

The utility of linear theory as a vehicle with which one might accurately assess whether an unstable flow might effectively radiate IGWs was cast into considerable doubt by the analysis of McIntyre and Weissman (1978), who pointed out that the penetration depth of a small amplitude incipient disturbance into a region of constant horizontal velocity and Brunt–Väisälä frequency is inversely proportional to the growth rate of the disturbance during its linear phase of development. They therefore suggested that a rapidly growing instability may only give rise to waves that intrude weakly into the surrounding medium and strongly penetrating waves can only arise from a weakly growing disturbance. In either circumstance, it was therefore suggested, an understanding of the nonlinear development of the flow would seem to be necessary to determine whether significant IGW radiation could occur. Several possible nonlinear mechanisms have since been proposed to account for observations of IGW radiation including wave excitation through vortex pairing (Davis and Peltier 1979) and through wave–wave interactions, a mechanism that has often been referred to as involving envelope radiation (Fritts 1982; Fritts 1984; Chimonas and Grant 1984). However, none of these mechanisms appear to constitute a source that could be responsible for generating waves of sufficiently large amplitude to account for the momentum deposition associated with wave-induced turbulence in the lower stratosphere.

Recently, however, the preconditions of the basic state necessary for direct coupling between the most unstable mode and a propagating wave in the far field were more fully analyzed by Sutherland and Peltier (1994), who showed through the application of high-resolution nonlinear numerical simulations that large amplitude IGWs are excited when N^2 is sufficiently small in the region of maximum shear and N^2 is sufficiently large in the far field where the background velocity is constant. (An N^2 profile of this kind is referred to hereafter as possessing an "N^2 notch.") In these circumstances, waves may be generated directly by way of a shear instability mechanism independently of whether or not a lower boundary is present. On the basis of linear theory, some authors [i.e., Lindzen and Barker (1985); Lott et al. (1992)] have previously considered the possibility for IGW generation by shear instability in mean flows with an N^2 notch but they have not addressed the question of whether significant wave emission would in fact be realized in the presence of nonlinear interactions between the growing instability and the mean flow. A new and, we believe, generic approach to the problem of shear excitation of IGWs has been suggested by Sutherland et al. (1994), who have reevaluated the analyses of McIntyre and Weissman (1978) and thereby demonstrated that a "penetration condition" can in fact be constructed that successfully predicts, on the basis of linear theory, whether a stratified parallel flow may effectively radiate waves as a direct consequence of shear instability. This analysis has also demonstrated that such emission can be extremely intense and has defined the circumstances that make it possible. The predictions of the penetration condition have been supported by the results of nonlinear simulations in which strong and continuous IGW radiation with the same phase speed and horizontal wavelength as the most unstable mode of linear theory has been observed (Sutherland and Peltier 1994; Sutherland et al. 1994).

The question remains, however, as to whether the circumstances necessary for this emission process to operate are in fact realizable in the earth's atmosphere. In partial answer, we examine herein the excitation of IGWs by a model tropospheric jet stream that is assumed to be driven to shear instability by a process that forces the jet maximum to a lower than normal elevation in such a way that the upper flank of the jet lies beneath the tropopause.

Some indirect evidence, which seems to indicate that this mechanism for the generation of IGWs may in fact occur in the atmosphere, is found by comparing the

observations of mean zonal winds in the lower and middle atmosphere with the results of general circulation models (GCMs), which presently exhibit a westerly bias in their ability to reproduce the meridional profiles of Southern Hemispheric mean zonal winds during the Northern Hemisphere summer (Boer et al. 1992). This deficiency is illustrated in Fig. 1. In Fig. 1a the three-year average of the mean zonal winds for both hemispheres are shown for Northern Hemisphere summer according to the results from the CIRA-86 model (Manson et al. 1991). Figure 1b shows a schematic of the June, July, and August average zonal winds calculated in the GCMs. The winds shown below 50-mb pressure are based on those shown in Fig. 9 of McFarlane et al. (1992), and the winds shown above 50 mb are those typical of some prerelease GCMs, which

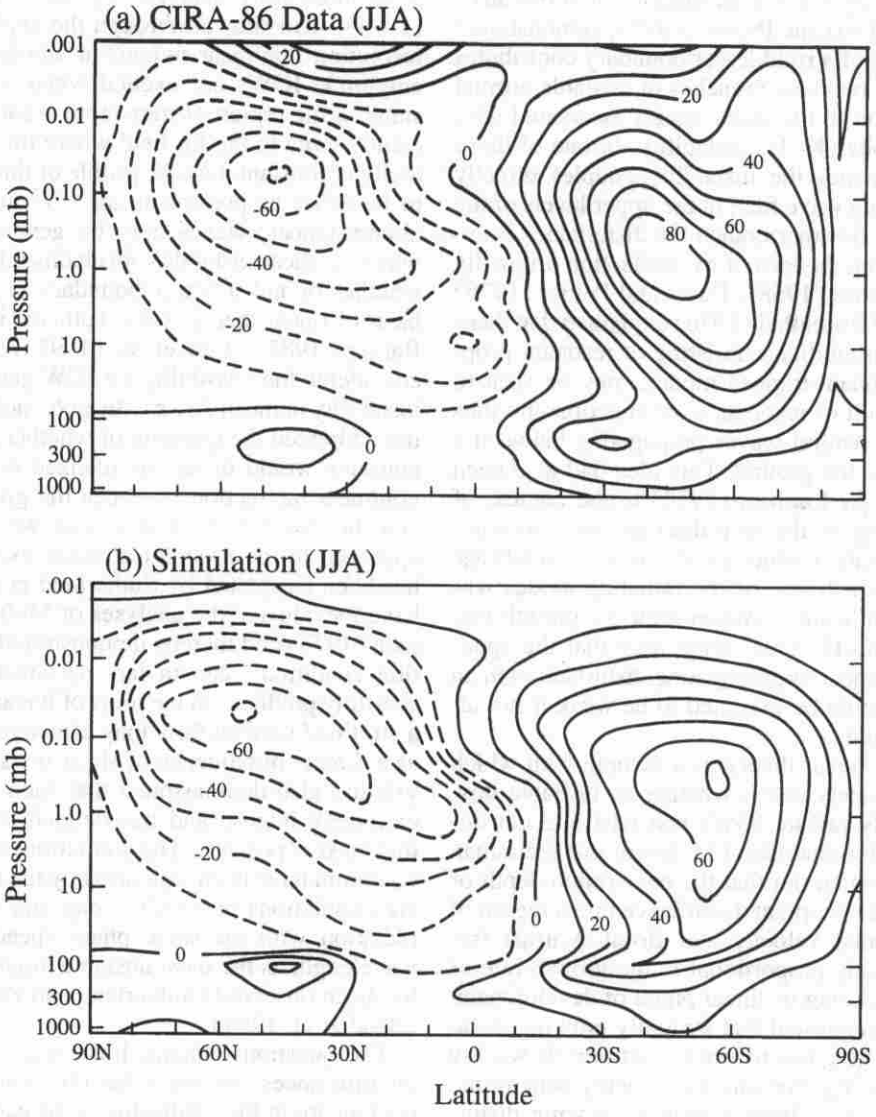

FIG. 1. Comparison of observations with GCMs: meridional profiles of average zonal velocity time averaged over June, July, and August (a) taken from CIRA-86 model and (b) schematically represented from the Canadian Climate Centre GCM below 50 mb (McFarlane et al. 1992) and some prerelease versions of models of the middle atmosphere. GCMs parameterize the effects of wave drag due to topographic forcing, and the zonal winds reproduced in such simulations compare reasonably well with observations in the Northern Hemisphere. The simulated zonal winds associated with the peak of the tropospheric jet in the Southern Hemisphere, however, are about 20%–30% stronger than the observed maximum wind speed, and the observed closure of the jet in Southern Hemisphere winter is difficult to reproduce. The model stratospheric winds in the Southern Hemisphere tend to be too weak. Both deficiencies could conceivably be accounted for if the shear generation of IGWs from the top flank of the tropospheric jet does in fact occur.

model the middle atmosphere. Although the horizontal grid scale of the model is too large to capture the dynamics of IGWs with horizontal wavelengths less than about 50 km, a gravity wave drag parameterization scheme is employed in the model (McFarlane 1987) that attempts to capture the effect of waves generated by topographic forcing and breaking in the middle atmosphere according to criteria described by Lindzen (1981) but based upon the analyses of topographic internal wave breaking by Peltier and Clark (1979, 1980). However, because the tropospheric jet stream in the Southern Hemisphere flows almost entirely over oceans, very little wave drag is imposed by the parameterization scheme in this region. The maximum zonally averaged wind speed of the Southern Hemisphere tropospheric jet stream in the model is near 40 m s^{-1}, which is 20%–30% greater than the average maximum wind speed observed in July. Furthermore, the simulated jet is only weakly closed, a feature that is also discordant with observations, therefore implying that the model neglects a significant source of drag, presumably due to wave momentum transport at unresolved scales. The mechanism we herein propose for IGW generation by the jet stream is therefore appealing in two ways. Not only might large amplitude IGWs generated in the troposphere be available thereafter for momentum deposition in the middle atmosphere, but the tropospheric jet itself would also be decelerated by the wave emission process. Hence the strength of the Southern Hemispheric jet stream may be overpredicted, not because there is inadequate *absorption* of counterflow momentum that would accompany wave breaking at the elevation of the jet stream, but rather because *emission* of internal waves from the jet is not properly accounted for. Because there is very little variation of topography at the latitude of the Southern Hemispheric jet stream, the former explanation is untenable on a priori grounds, suggesting than an alternative hypothesis is required. It may be that the reason the alternative hypothesis presented herein has not been previously explored is that the paper of McIntyre and Weissman (1978) is assumed to exclude it. As has been shown in detail by Sutherland et al. (1994), however, the McIntyre and Weissman analysis cannot be construed to rule out this possibility.

In order to more clearly illustrate the distinction between gravity wave drag arising from the emission of radiation that is the central idea of this paper and the conventional case of gravity wave drag as arising from the absorption of momentum whose flux is maintained by upward propagating waves, a schematic illustration is provided in Figs. 2. The left-hand diagram illustrates the conventional mechanism for wave drag (indicated by the large left-going arrow), wherein topographically generated stationary upward propagating IGWs deposit their momentum at a level where the waves break. In contrast, the right-hand diagram illustrates the excitation of IGWs from a dynamically unstable shear layer.

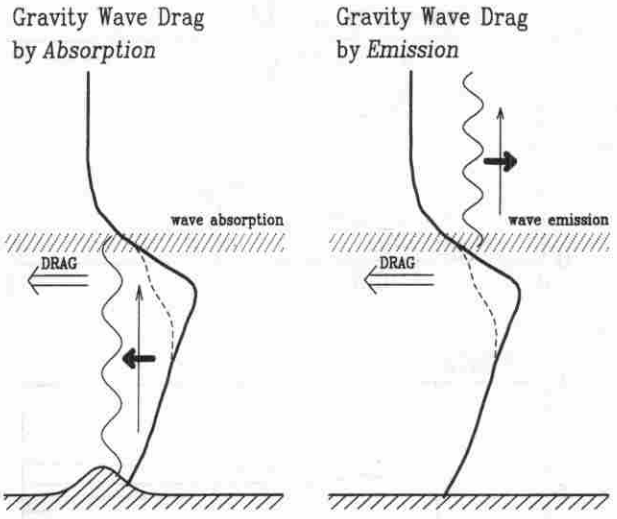

FIG. 2. The schematic represents two mechanisms by which IGWs may exert drag on a jet flow. The left-hand diagram demonstrates a mechanism for wave drag via wave absorption in the presence of topography and an upper critical layer. The right-hand diagram demonstrates a mechanism for wave drag via wave emission in a dynamically unstable flow that is shear unstable on the upper flank of the jet. Double horizontal arrows indicate the direction of wave drag. The thick solid curve is a profile of the mean flow for the tropospheric jet stream, and the thin dashed curve illustrates the state to which the mean flow evolves under the decelerating influence of wave drag. Thin vertical arrows indicate the direction of wave energy propagation, and the overlapping thick horizontal arrows indicate the direction with respect to the mean flow of the horizontal momentum that is transported vertically upward by the waves. Note that the absorption of waves vertically transporting upstream momentum exerts drag in the same direction as the emission of waves vertically transporting downstream momentum.

Waves generated in this manner propagate upward and downstream. Of course these waves may act so as to accelerate the mean flow at a critical level situated above the level of generation, but the significant observation here is that the mean flow is decelerated as a result of the reaction of the mean flow to the emission of radiation that transports streamwise momentum upward. This paper is devoted to the development of the idea that this process is both fluid mechanically possible and plausibly of great importance to the understanding of the detailed structure of the large-scale dynamical state of the earth's atmosphere.

After describing the nonlinear model to be employed in our analyses in section 2 we present the results of a series of two-dimensional nonlinear simulations in section 3, which are initialized with profiles of $N^2(z)$ characteristic of the atmosphere and of $U(z)$ representing the tropospheric jet perturbed by external forcing so that the maximum shear on the upper flank of the jet obtains at an elevation where $N^2(z)$ has typical tropospheric rather than stratospheric values. We examine in detail the effect of varying the strength of the shear on the vertical flux of horizontal momentum associated

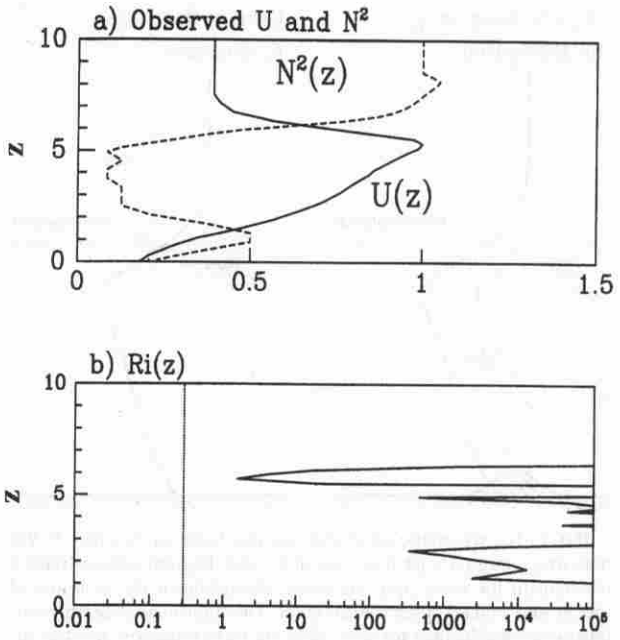

FIG. 3. Nondimensional profiles of horizontal velocity $U(z)$ and squared Brunt–Väisälä frequency $N^2(z)$ taken from observations by Lilly and Zipser (1972) upstream of a downslope windstorm. The maximum velocity $\mathcal{U} = 51.2$ m s^{-1}, the half width of the upper flank of the jet $\mathcal{L} = 1.7$ km, and the bulk Richardson number $J = 0.66$ define characteristic scales used to nondimensionalize the flow parameters.

with the waves and the contribution that the emission of the waves makes to the stabilization of the flow.

2. Background

In order that the results of this study may be more easily compared with those pertaining to a more general class of flows, we shall present them in an appropriately nondimensional form. In this nondimensionalization we shall represent the quantities of length (x_*, z_*), velocity (u_*, w_*), time (t_*), and potential temperature (θ_*) as

$$(x, z) = \frac{1}{\mathcal{L}}(x_*, z_*), \quad (u, w) = \frac{1}{\mathcal{U}}(u_*, w_*),$$

$$t = \frac{\mathcal{U}}{\mathcal{L}} t_*, \quad \theta = \frac{1}{\Theta_0}\theta_*, \quad (1)$$

in which the characteristic length scale $\mathcal{L}$ is defined to be the half-width of the jet on its upper flank, the characteristic velocity scale $\mathcal{U}$ is the maximum speed of the jet, and Θ_0 is the surface potential temperature.

To support the plausibility of the analysis we shall perform, the basic-state vertical profiles of mean horizontal velocity $U(z)$ and squared Brunt–Väisälä frequency $N^2(z)$, which will be employed to initialize the nonlinear simulations, have been derived from a specific set of observations by Lilly and Zipser (1972) [see also Lilly and Kennedy (1973)] of the lower atmosphere during the downslope windstorm that occurred near Boulder, Colorado, on 11 January 1972. The nondimensional profiles of U and N^2 upstream of the region where the windstorm occurred are shown in Fig. 3a, and the values of the characteristic scales extracted from the dimensional profiles are summarized in Table 1.

Since it is the wave generation process that is of interest here, it is sufficient to assume that $U(z)$ and $N^2(z)$ are constant at high altitudes. The bulk Richardson number is defined by $J = (\mathcal{L}^2/\mathcal{U}^2)N_*^2 = (g/\mathcal{H})(\mathcal{L}/\mathcal{U})^2$, in which N_* is the observed (dimensional) Brunt–Väisälä frequency in the lower stratosphere. We set $J = 0.66$ and $N^2(z) = 1$ for large z in the nondimensional representation of the squared Brunt–Väisälä frequency. The density-scale height $\mathcal{H}$ corresponding to this value of J is 16.4 km, which is significantly larger than $\mathcal{L}$ and is consistent with the Boussinesq approximation.

The gradient Richardson number $\mathrm{Ri}(z)$ corresponding to the observed profiles of U and N^2 is shown in Fig. 3b. According to the Miles–Howard theorem (Miles 1961; Howard 1961), because $\mathrm{Ri}(z)$ is greater than 1/4 for all z, the flow is stable to normal mode disturbances. However, through external forcing by such factors as bottom topography or the development of frontal systems, the basic state may change so that the gradient Richardson number becomes less than 1/4 over some range of z, in which case the potential for instability exists. Though a robust class of perturbed jet flows appear to be unstable and capable of generating large-amplitude IGWs, in this study we shall fix the altitude z_0 of the shear on the upper flank of individual jet flows and then examine the effect of varying the shear half-depth R_0 on the mechanism by which IGWs are excited and radiate upward into the stratosphere.

In the specific cases to be discussed below, analytic approximations are made to the observed basic-state

TABLE 1. Dimensional scales and nondimensional parameters used to define initial vertical profiles of horizontal velocity $\bar{U}(z)$ and squared Brunt–Väisälä frequency $N^2(z)$. Respectively, $\mathcal{U}$ and $\mathcal{L}$ are the maximum speed and half-width of the upper flank of the jet flow observed by Lilly and Zipser (1972) upstream of a downslope windstorm (see Fig. 3); $\mathcal{H}$ is the density-scale height determined from the vertical variation of background density in the lower stratosphere. The bulk Richardson number J is nondimensional.

Characteristic scales	$\bar{U}(z)$	$JN^2(z)$
$\mathcal{L} = 1.7$ km	$m_1 = 0.2$	$a_1 = 0.31$ $a_2 = 0.31$ $a_3 = 0.35$
$\mathcal{U} = 51.2$ m s^{-1}	$U_0 = 0.2$	$z_1 = 0.31$ $z_2 = 1.0$
$\mathcal{T} = \mathcal{L}/\mathcal{U} = 33$ s	$U_\infty = 0.39$	$R_1 = 0.6$ $R_2 = 1.0$
$\mathcal{H} = 16.4$ km		
$\mathcal{J} = 0.66$		

profiles shown in Fig. 3a according to the representations

$$U(z) = \frac{m}{2}(z - z_a)\left[1 - \tanh\left(\frac{z - z_0}{R_0}\right)\right] + U_\infty \quad (2)$$

and

$$JN^2(z) = a_1 \tanh\left(\frac{z - z_1}{R_1}\right) + a_2 \operatorname{sech}^2\left(\frac{z - z_2}{R_2}\right) + a_3, \quad (3)$$

in which $J = a_1 + a_3$. The parameters in (2) and (3) are also listed in Table 1. These completely specify $N^2(z)$ and they specify $U(z)$ with two variable parameters z_0 and R_0, which determine the altitude and half-depth of the shear layer on the top flank of the jet, respectively. Given z_0 and R_0, the parameter z_a is determined by requiring on the basis of the observed horizontal velocity profile that the surface wind speed is U_0 (= 0.2) and the surface shear is $U'(z = 0) = m_1$ (= 0.2). Both $N^2(z)$ and $U(z)$ are constant for large z, a feature uncharacteristic of the atmosphere but which is useful in these simulations to clearly demonstrate that upward propagating waves exhibit the properties of plane IGW.

From the basic-state profiles, the most unstable mode of linear theory is determined through the application of a Galerkin stability analysis employing finite Reynolds number (Re) and Prandtl number (Pr) [e.g., Klaassen and Peltier (1985)]. This analysis is performed for domains of sufficient height and with sufficiently high resolution that predicted growth rates are relatively insensitive to any further increase in either of these quantities. As an additional check on the accuracy and insensitivity of the initial instability to these high values of Re and Pr, the linear stability of an inviscid flow is examined independently by solving the Taylor–Goldstein equation using a shooting method previously described in Sutherland and Peltier (1992). For each basic state that we have examined, the horizontal wavelength, phase speed, and growth rate of the most unstable mode determined by the shooting method are found to be within 2% of the values calculated by the Galerkin method for Re = 1000, 2000, and 4000.

Applying the penetration condition proposed by Sutherland et al. (1994), it is possible to assess whether IGWs may radiate upward into the far field, where $N^2(z) = 1$ and $U(z) = U_\infty$ are constant. To this end, the penetration ratio $\mathcal{D}$ is defined to be the product of the vertical wavenumber γ_r and the penetration depth $1/\gamma_i$ of the mode in the far field, where γ_r and γ_i are the real and imaginary parts, respectively, of the complex vertical wavenumber γ determined from the Taylor–Goldstein equation

$$\phi_{zz} + \gamma^2\phi = 0, \quad (4)$$

in which $\phi(z)$ is the streamfunction amplitude and in the far field

$$\gamma^2 = +\frac{J}{(U_\infty - c_p)^2 - \alpha^2}, \quad (5)$$

in which α is the horizontal wavenumber and c_p is the (possibly complex) horizontal phase speed. This last expression is just the dispersion relationship for growing as well as for neutrally propagating disturbances, as clearly demonstrated by rearranging terms in (5):

$$\Omega^2 = \frac{J\alpha^2}{(\alpha^2 + \gamma^2)}, \quad (6)$$

in which $\Omega = \alpha(c_p - U_\infty)$ is the Doppler-shifted frequency of the wave with respect to the background flow in the far field. The penetration ratio may be reexpressed in terms of the growth rate σ and phase speed so that

$$\mathcal{D}^2 - 2\mathcal{B}\mathcal{D} - 1 = 0, \quad (7)$$

in which

$$\mathcal{B} = \frac{1}{2}\frac{1}{\Omega\sigma}\left[\frac{1}{J}(\Omega^2 + \sigma^2)^2 - \Omega^2 + \sigma^2\right]. \quad (8)$$

In this way, the penetration ratio is easily calculated from the most unstable mode characteristics. The penetration condition predicts that waves should be excited directly by the growth of the most unstable mode if $|\mathcal{D}| > 1$. The critical value of the penetration ratio $|\mathcal{D}| = 1$ is inferred on the basis of the following argument. McIntyre and Weissman (1978) proposed what they designated as a phase speed condition that asserted, in the notation used here, that IGWs with Doppler-shifted frequency $|\Omega_r| > J^{1/2}$ are evanescent in the far field, and this is entirely consistent with our penetration condition since $|\mathcal{D}| < 1$ if $|\Omega_r| > J^{1/2}$; if, on the other hand, $|\Omega_r| < J^{1/2}$ and $|\mathcal{D}| < 1$, then IGW may propagate, but the form of the wavepacket is determined by the growth and nonlinear saturation of the initial instability, and the applicability of linear theory in this case is cast into doubt. The penetration condition therefore stipulates that the properties of an IGW wavepacket generated by shear instability may be determined by linear theory if the most unstable mode is sufficiently "wavelike" in the far field, where by sufficiently wavelike we mean that there is more than one wavelength of the wave within a single *e*-folding depth of the amplitude. We will show that nonlinear simulations are highly consistent with the predictions of the penetration condition defined in this way.

The nonlinear simulations are performed by numerically solving the primitive equations for incompressible, Boussinesq flow that is restricted to two spatial dimensions. These are represented numerically in a model based on the methodology developed by Smyth and Peltier (1989) for the study of the evolution of

Kelvin–Helmholtz and Holmboe waves. The nondimensional form of the fully nonlinear equations for momentum conservation and for the conservation of internal energy are, respectively:

$$\frac{Du}{Dt} = -p_x' + \frac{1}{\mathrm{Re}}\nabla^2 u \tag{9}$$

$$\frac{Dw}{Dt} = -p_z' - J\rho' + \frac{1}{\mathrm{Re}}\nabla^2 w \tag{10}$$

and

$$\frac{D\rho'}{Dt} = N^2 w + \frac{1}{\mathrm{RePr}}\nabla^2\rho', \tag{11}$$

in which $D/Dt = \partial/\partial t + \mathbf{u}\cdot\nabla$ is the material derivative. The Reynolds number is $\mathrm{Re} = \mathcal{U}\mathcal{L}/\nu$ in which ν is the kinematic viscosity, whereas the Prandtl number is $\mathrm{Pr} = \nu/\kappa$ in which κ is the thermal diffusivity. The pressure fluctuation p' is the total pressure minus the pressure $\bar{p}(z)$ that is in hydrostatic balance with the background density $\bar{\rho}(z)$. In the Boussinesq approximation, both the background and fluctuation density are represented nondimensionally by $\rho = (\mathcal{H}/\mathcal{L})(\rho_*/\rho_0)$, in which ρ_* is the density in dimensional variables and ρ_0 is the dimensional surface density. The domain is assumed to be a horizontally periodic channel with free-slip upper- and lower-boundary conditions.

Rather than integrate (9)–(11), it is convenient to reexpress these equations in vorticity–streamfunction form, since the model then reduces to the evolution equations for only two coupled fields, namely ω and ρ'. Taking the curl of (9) and (10) gives the vorticity equation

$$\frac{D\omega}{Dt} = J\rho_x' + \frac{1}{\mathrm{Re}}\nabla^2\omega, \tag{12}$$

in which $\omega = u_z - w_x$ is the spanwise component of vorticity. The streamfunction is found by inverting the elliptic differential equation

$$\nabla^2\psi = -\omega, \tag{13}$$

and from ψ the components of the velocity vector may be determined.

To solve the model equations, the fields ω and ρ' are decomposed into horizontal spectral components, and vertical derivatives are represented using a second-order accurate centered finite-difference scheme. Time stepping is achieved through application of the second-order accurate leapfrog scheme, with an Euler backstep taken at regular intervals to eliminate splitting errors. To ensure that the results are not sensitive to resolution, simulations were performed for channels of varying width, and the model equations were integrated with varying spatial and temporal resolution.

Diffusion in the model is enhanced at small scales to a degree that is determined by the Reynolds number and the Prandtl number. The simulations to be described here are performed with moderately high Reynolds number $\mathrm{Re} = 2000$ and with $\mathrm{Pr} = 1$. In simulations performed with $\mathrm{Re} = 1000$ and 4000 (not discussed in detail here), the qualitative features of the flow evolution were observed to be relatively insensitive to Re at these high values.

The most unstable mode, which is normalized so that the maximum (nondimensional) vertical velocity of the perturbation is initially set to be w_0 (typically 0.05), is superposed on the background fields of density and horizontal velocity, and a small amplitude random component is added across the wavenumber spectrum. The horizontal extent of the domain is set to allow the growth of precisely one wavelength of the most unstable mode.

During the initial stages of nonlinear development of the flow, the predicted growth rate σ of the most unstable mode is compared to the initial growth rate σ_0 of the perturbation determined in simulations by examination of the initial change in perturbation energy E'. Specifically, σ is compared with $\sigma_0 = (1/2E')(dE'/dt)$ and, in practice, agreement is generally found to within five percent.

As the flow develops nonlinearly, diagnostic analyses are applied to ensure that momentum conservation is maintained between the mixing region and the far field and also to examine the extent to which the radiating waves in the far field act to stabilize the mean flow in the mixing region. The mathematical details of these methods are presented here.

Throughout each simulation the time rate of change of mean horizontal momentum is compared with the momentum change due to diffusion of the mean flow and due to the Reynolds stress divergence. In the Boussinesq approximation the (nondimensional) zonally averaged horizontal momentum is $\bar{u}(z)$. From (9) the prognostic equation for $\bar{u}$ is

$$\frac{\partial\bar{u}}{\partial t} = -\frac{\partial}{\partial z}\bar{\tau} + \frac{1}{\mathrm{Re}}\frac{\partial^2}{\partial z^2}\bar{u}, \tag{14}$$

in which $\tau = (u - \bar{u})(w - \bar{w})$ is the Reynolds stress that measures the vertical flux of horizontal momentum by waves and the overbar denotes horizontal averaging. The rate of change of $\bar{u}$ between two vertical levels z_1 and z_2 is given by integrating equation (14) over this range. Denoting the vertical integral of $f(z)$ by the notation $\langle f\rangle_z$,

$$\frac{\partial\langle\bar{u}\rangle_z}{\partial t} = -[\tau(z_2) - \tau(z_1)] + \frac{1}{\mathrm{Re}}\left[\frac{d\bar{u}(z_2)}{dz} - \frac{d\bar{u}(z_1)}{dz}\right]. \tag{15}$$

For each nonlinear simulation to be discussed below, the change of momentum due to Reynolds stress divergence and diffusion of the mean flow is calculated over regions denoted by $\mathcal{R}_1$, $\mathcal{R}_2$, and $\mathcal{R}_3$, corresponding

to the vertical ranges $0 \leq z \leq z_0$, $z_0 \leq z \leq z_t$, and $z \geq z_t$, respectively. Here z_0, which is a parameter in (2) determining the initial mean-flow profile, corresponds approximately to the inflection point on the upper flank of the jet and also to the vertical position of the minimum gradient Richardson number. The boundary separating $\mathcal{R}_2$ and $\mathcal{R}_3$ at $z = z_t$ is set to represent a vertical level that is close to the mixing region but sufficiently far above z_0 that there is negligible diffusion of the mean flow into $\mathcal{R}_3$ and no convective overturning in $\mathcal{R}_3$. In this study we somewhat arbitrarily set $z_t = 10$. In $\mathcal{R}_3$, $U(z) \approx U_\infty$ and $N^2(z) = 1$ may be treated as constant. During the process of stabilization of the mean flow, momentum is transferred either by diffusive processes or by wave momentum flux from $\mathcal{R}_1$ to $\mathcal{R}_2$ and $\mathcal{R}_3$, though in simulations with Re = 2000 and 4000 it is found that the momentum change in $\mathcal{R}_3$ is attributed primarily to the momentum flux associated with IGWs.

The vertical redistribution of horizontal momentum by Reynolds stress provides a useful characterization of the process of stabilization of the mean flow. For the time and length scales characteristic of the real tropospheric jet, the Reynolds number is at least of the order $\mathrm{Re} \approx 10^9$, and so molecular diffusion should not contribute significantly to the relaxation process of a strongly perturbed unstable flow. Stabilization takes place either through enhanced diffusion by turbulent mixing of eddies or through vertical transport of momentum away from the mixing region by IGWs. In the former process momentum is locally redistributed in the mixing region, reducing the shear strength and increasing the gradient Richardson number to a value greater than 1/4. In the latter process momentum is entirely removed from the mixing region. Under geophysical circumstances in which large amplitude IGW are excited, the stabilization of the tropospheric jet should involve some combination of these local and nonlocal processes both of which, at sufficiently high Reynolds number, may be characterized by the Reynolds stress.

In simulations it is found that the vertical position $z \approx z_0$ of the uppermost inflection point of the mean flow varies little throughout the nonlinear evolution of the flow. The total wave momentum transport across z_0, M_T, is given by the time integral of the Reynolds stress at z_0, which is continuously calculated throughout the stabilization process. In the absence of molecular diffusion, this is a measure of the mean-flow momentum redistribution (both local and nonlocal) that is necessary to reduce the shear and stabilize the flow. The time integral of the Reynolds stress calculated continuously at a vertical level $z = z_t$ is used to give a measure of the total (nonlocal) redistribution of momentum by IGWs, M_W. We therefore characterize the degree to which the mechanism of IGW radiation contributes to the stabilization of the mean flow by the ratio $\mathcal{S} = -M_W/M_T$, which is zero if the mechanism does not contribute and which is unity if the mechanism is entirely responsible for the stabilization process.

In each simulation the energy content, phase tilt, and vertical group velocity of the waves are examined in $\mathcal{R}_3$ where N^2 and U are constant. According to linear theory, the energy of plane IGWs propagating in this region should be equally partitioned between kinetic energy (KE) and available potential energy (APE) forms [e.g., Gill (1982) §7.8]. Denoting horizontal averaging by an overbar, the mean KE is defined by

$$\overline{\mathrm{KE}} = \frac{1}{2}(\overline{u'^2} + \overline{w'^2}), \tag{16}$$

and the mean APE is defined by

$$\overline{\mathrm{APE}} = \frac{1}{2} J \overline{\rho'^2}, \tag{17}$$

in which $u' = u - \bar{u}$, $w' = w - \bar{w}$, and $\rho' = \rho - \bar{\rho}$.

The local phase tilt of the waves with the vertical, Θ_γ, may be calculated at an altitude where the Reynolds stress is largest at the leading edge of the wavepacket. The phase tilt is given by

$$\Theta_\gamma = \arctan(\gamma/\alpha), \tag{18}$$

in which the vertical wavenumber γ is given approximately by

$$\gamma \approx \frac{d}{dz} \arctan\left[\frac{\mathrm{Im}(\rho_1)}{\mathrm{Re}(\rho_1)}\right] \tag{19}$$

and $\rho_1(z)$ is the (complex) amplitude of the perturbation density for the wave of the same horizontal extent as the initial normal mode disturbance. Θ_γ may be compared with the phase tilt expected from linear theory. From the dispersion relationship for IGWs, the phase tilt of the waves with intrinsic frequency Ω and horizontal phase speed c_p is

$$\Theta_\Omega = \arccos\left[\frac{\Omega}{(J)^{1/2}}\right]. \tag{20}$$

Likewise, the horizontal phase speed $c_p^{(\theta)}$ of plane IGWs may be inferred from the phase tilt of the waves: $c_p^{(\theta)} = [(J)^{1/2}/\alpha] \cos(\Theta_\gamma)$. If the waves are excited directly through coupling with the most unstable normal mode, then this should equal the phase speed of the initial instability.

If the intrinsic frequency Ω of the most unstable mode is less than the Brunt–Väisälä frequency, the speed at which the wavepacket moves upward may be estimated on the basis of linear theory by the vertical group velocity:

$$c_{gz} = (c_p - U_\infty) \cos^2\Theta_\Omega \sin\Theta_\Omega. \tag{21}$$

In the simulations to be discussed below, the application of these diagnostics gives convincing evidence that fluctuations excited by the unstable jet are indeed

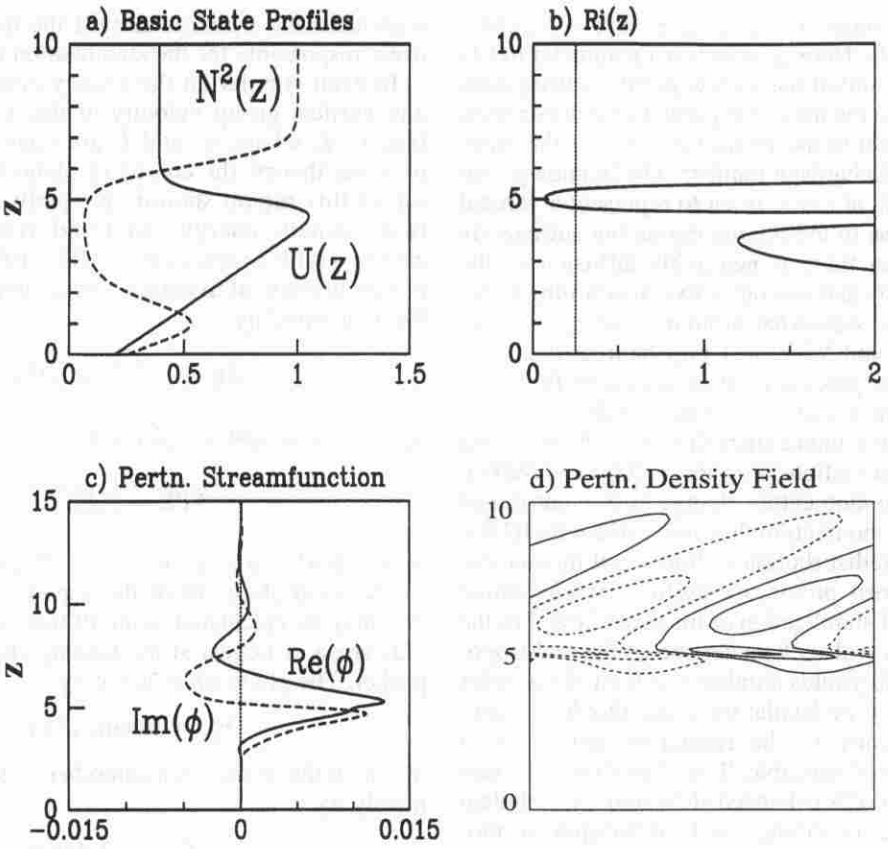

FIG. 4. Initial state for case 1 showing (a) profiles of $U(z)$ and $N^2(z)$ (nondimensional), (b) the gradient Richardson number for this basic state, (c) the real (solid) and imaginary (dashed) parts of the perturbation streamfunction amplitude of the most unstable normal mode, and (d) contours of the perturbation density field (contour interval is 0.01) corresponding to this mode. The undulations and phase tilt of the disturbance in the region above the jet indicate that the most unstable mode couples directly with the IGW field.

IGWs and that, in the case of continuously excited waves, the horizontal wavelength and phase speed of the waves are determined from the most unstable mode calculated in linear theory.

3. Results from the nonlinear simulations

The profiles of $U(z)$ for $z_0 = 5.0$ and $R_0 = 0.4$, and of $N^2(z)$, are shown in Fig. 4a. In dimensional units these parameters correspond to a jet profile such that the maximum shear on the top flank of the initial tropospheric jet occurs at $(z_0)_* \approx 8.5$ km and the half-depth of the region of strong shear is $(R_0)_* \approx 0.7$ km. The gradient Richardson number profile corresponding to this basic state is shown in Fig. 4b and indicates that the flow may admit the growth of a normal mode disturbance driven by shear instability on the top flank of the jet where $\mathrm{Ri}(z) < 1/4$. Indeed, a Galerkin linear stability analysis applied to this basic state with Re = 2000 demonstrates that the flow is unstable and the characteristics of the most unstable mode are listed in Table 2. From the growth rate, phase speed, and horizontal wavenumber of this mode, the penetration ratio is determined to be $|\mathcal{D}| \approx 2.56 > 1$, and the flow is therefore expected to radiate IGWs upward into the stratosphere. This relationship is demonstrated explicitly in Fig. 4c, which shows the real and imaginary parts of the perturbation streamfunction amplitude corresponding to the most unstable mode: the out-of-phase undulations of the mode in the upper region undergo many oscillations over an e-folding depth, and this structure, presumably, should persist as the flow develops nonlinearly. The initial perturbation density field corresponding to the normal mode is shown in Fig. 4d and further demonstrates the direct coupling of the instability with the internal wave field in the upper levels. The downstream phase tilt is characteristic of upward propagating waves with positive horizontal phase speed with respect to the background flow. As the flow develops nonlinearly from this initial state, the waves grow in amplitude while extending further upward into the stratosphere.

TABLE 2. Characteristics of the most unstable mode are tabulated for three different simulations. In each case Re = 2000. Nondimensional quantities listed are the horizontal wavenumber (α), the growth rate (σ), horizontal phase speed (c_ρ), and vertical group velocity (c_{gz}) of waves well above the jet. Dimensional quantities, which are listed in parentheses, are the horizontal wavelength ($\lambda = 2\pi/\alpha$) and e-folding time ($1/\sigma$) for disturbance growth. The penetration ratio ($\mathcal{D}$) is the product of the vertical wavenumber and the penetration depth of the extension of the most unstable mode into the upper region in which the basic-state profiles are constant. In the two cases for which $|\mathcal{D}| > 1$ the phase tilt and vertical group velocity of the waves in the upper region are predicted. Characteristic scales for conversion from nondimensional to dimensional parameters are given in Table 1.

Characteristic	Case 1 $z_0 = 5.0$, $R_0 = 0.4$	Case 2 $z_0 = 5.0$, $R_0 = 0.3$	Case 3 $z_0 = 5.0$, $R_0 = 0.2$
α	1.74	1.93	2.40
wavelength	(6.1 km)	(5.5 km)	(4.5 km)
σ	0.098	0.180	0.313
e-folding time	(5.6 min)	(3.1 min)	(1.8 min)
c_ρ	0.755	0.755	0.760
$\lvert\mathcal{D}\rvert$	2.56	1.17	0.45
Θ_Ω	38.7°	29.9°	N/A
c_{gz}	0.139	0.137	N/A

The nonlinear development of the vorticity field is shown at times 100 and 200 in Figs. 5a and 5b, respectively. Only the region for $0 \leq z \leq z_t$ is displayed to emphasize that the small-scale features of the flow are well resolved. The perturbation density field, which is shown for the full domain at times 100 and 200 in Figs. 5c and 5d, respectively, clearly demonstrates the upward vertical propagation of a wavepacket that is generated at low levels by large-scale fluctuating disturbances in the tropospheric jet. At time 100, the downstream-tilting waves are apparently excited by the undulating motion of the upper flank of the jet, which results from the nonlinear development of the most unstable mode. At time 200, the flow has nearly stabilized due to mixing in the jet and also, as we will show, due to the significant extraction of horizontal momentum by upward propagating waves. The flow at this time is predominantly parallel, and waves are only weakly generated. For times $t \geq 224$ (about 2 h) the minimum gradient Richardson number, which is calculated from the horizontally averaged profiles of U and N^2, is greater than 1/4. The low-level flow is predominantly parallel and stable after this time.

To determine the degree to which the characteristics of the propagating wavepacket in the upper region are similar to the properties of plane IGWs, we apply the diagnostics described in section 2, the results of which are listed in Table 3. At the leading edge of the upward propagating wave ($t = 100$) the ratio APE:KE is calculated where KE is largest ($z \approx 18.2$). This ratio equals 1.04, which is close to unity, the ratio expected for plane IGWs for which APE and KE are in equipartition. At this altitude the phase lines of the waves tilt with an angle $\Theta_\gamma \approx 36.7°$ to the vertical, which compares well with the angle required by the dispersion relationship for IGW, namely $\Theta_\Omega \approx 38.7°$. Likewise, the phase speed of the waves inferred from Θ_γ is close to that of the most unstable mode, supporting the assertion that these waves are excited directly from the growth and development of the instability.

The Reynolds stress profiles shown at times $t = 100$ and 200 in Figs. 6a and 6b, respectively, indicate that a large upward vertical flux of horizontal momentum is associated with the continuously excited waves. By way of comparison, during intense downslope windstorm events the largest Reynolds stresses recorded are of the order 0.1–1 N m^{-2} [e.g., Palmer et al. (1986)]. In this simulation the largest Reynolds stress occurring at $z_t = 10$ is 0.0034 (0.92 N m^{-2}) at time $t = 52$ (29 min). Therefore, the wave momentum flux associated with our shear excitation mechanism may be as large as the momentum flux associated with topographic forcing. The broadening of the wavepacket and overall decrease of the peak values of Reynolds stress between times 100 and 200 is due primarily to dispersion effects. The transport of momentum away from the low-level jet is clearly seen in Figs. 6c and 6d, which show the mean flow at times $t = 100$ and 200, respectively. These are compared at both times with the horizontal velocity profile of the initial state (dashed curve). Momentum is extracted from the jet primarily between the upper inflection point at $z = z_0$ and the lower critical layer (where the mean-flow speed on the lower flank of the jet equals the speed of the flow at z_0). Indeed, the downward propagation of the instability acts to decelerate the jet, primarily near the lower critical layer where the disturbance is reabsorbed by the mean flow.

The stabilization of the flow by wave excitation is depicted in Fig. 7, which displays three graphs of the vertically integrated momentum changes $\Delta\tau_1$, $\Delta\tau_2$, and $\Delta\tau_3$ versus time due to wave momentum flux across the boundaries separating the three regions $\mathcal{R}_1$, $\mathcal{R}_2$, and $\mathcal{R}_3$, corresponding to $0 \leq z \leq z_0$, $z_0 \leq z \leq z_t$, and $z \geq z_t$, respectively, as previously mentioned. (Recall $z_0 = 5$ and $z_t = 10$.) As expected on the basis of momentum conservation considerations, the sum of these three curves at any instant of time must vanish. During the initial stages of flow development, momentum is transferred by waves from $\mathcal{R}_1$ to $\mathcal{R}_2$. A consequence of this transfer is that the strength of the shear at $z = z_0$ is reduced. As the momentum flux into $\mathcal{R}_2$ grows, so does the momentum flux into $\mathcal{R}_3$. Because only IGWs exist in $\mathcal{R}_3$, these waves irreversibly extract momentum from the mixing region and thereby contribute to the process of mean-flow stabilization.

The degree to which wave excitation contributes to the stabilization of the mean flow may be quantified in terms of a stabilization ratio $\mathcal{S} = -M_W/M_T$, which is the ratio of the total momentum flux across $z = z_t$ to the total momentum flux across $z = z_0$. From Table 3, $\mathcal{S} \approx 0.75$, indicating that about 3/4 of the momentum

that is redistributed from the mean flow below the inflection point on the top flank of the jet is associated with the upward emission of IGWs. This stabilization ratio is large but warrants more-detailed discussion. Firstly, in simulations of this case, with Re = 4000, the total momentum flux across z_t is found to be larger by approximately 40 percent. Nonetheless, $\mathcal{S}$ is larger by only 0.3 percent, so it appears that the ratio is relatively insensitive to the Reynolds number at these high values. Because the simulation is restricted to two dimensions, the mixing may be less intense than in a flow that is allowed to evolve freely in three dimensions. Implicit in this caveat is the notion that $\mathcal{S}$ could be somewhat overpredicted. On the other hand, the momentum flux across $z = z_t$ is greatest at $t = 52$ (about two eddy turnover times into the simulation) and, in accordance with Squire's theorem (Squire 1933), the growth of three-dimensional disturbances is not expected to be significant before this time. Therefore, a considerable quantity of momentum is expected to be transported in the vertical from the mean flow by the emission of IGW during the initial development of the two-dimensional flow.

TABLE 3. The results of diagnostic analyses applied to each nonlinear simulation. APE:KE is calculated at $t = 100$ (55 min) at a vertical level where the KE is greatest at the leading edge of the wavepacket. In dimensional units, max $\{\tau(z_t)\}$ is the largest value of the Reynolds stress at $z = z_t$ over the duration of the simulation. In all three cases this maximum occurs near time $t = 50$ (about 30 min). The stabilization ratio $\mathcal{S} = -M_W/M_T$ is a measure of the degree to which IGW radiation contributes to the stabilization of the mean flow as explained in detail in section 2.

Characteristic	Case 1	Case 2	Case 3
APE:KE	1.04	1.13	1.04
$c_p^{(\theta)}$	0.764	0.753	0.676
Θ_γ	36.7°	30.5°	32.2°
max $\{\tau(z_t)\}$	0.92 N (m^{-2})	1.46 N (m^{-2})	0.07 N (m^{-2})
$\mathcal{S}$	0.75	0.70	0.11

In case 2, we consider the evolution of a flow initialized with the same profile of $N^2(z)$ as in case 1 but

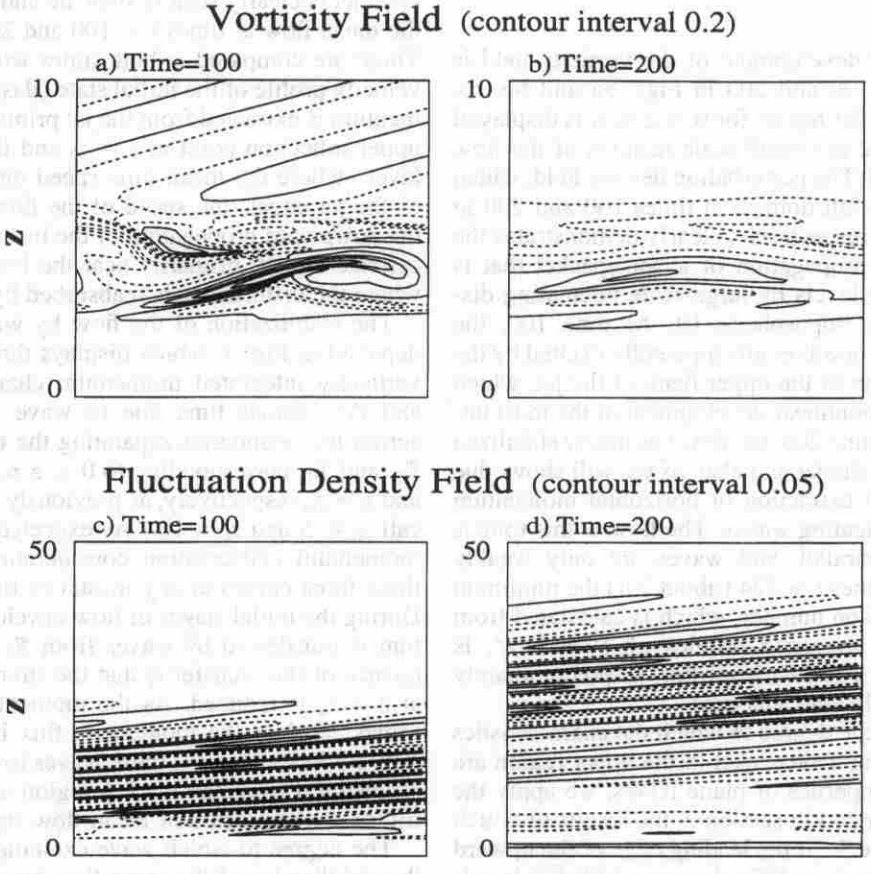

FIG. 5. From the simulation for case 1, contours of vorticity at times (a) $t = 100$ and (b) 200 and contours of perturbation density at times (c) $t = 100$ and (d) 200. Even after the flow evolves nonlinearly, waves continue to be excited by the large-scale features of the flow with the same horizontal extent as the initial instability. The wavepacket propagates upward in time with downstream phase tilt, and the jet eventually evolves to a stable parallel flow.

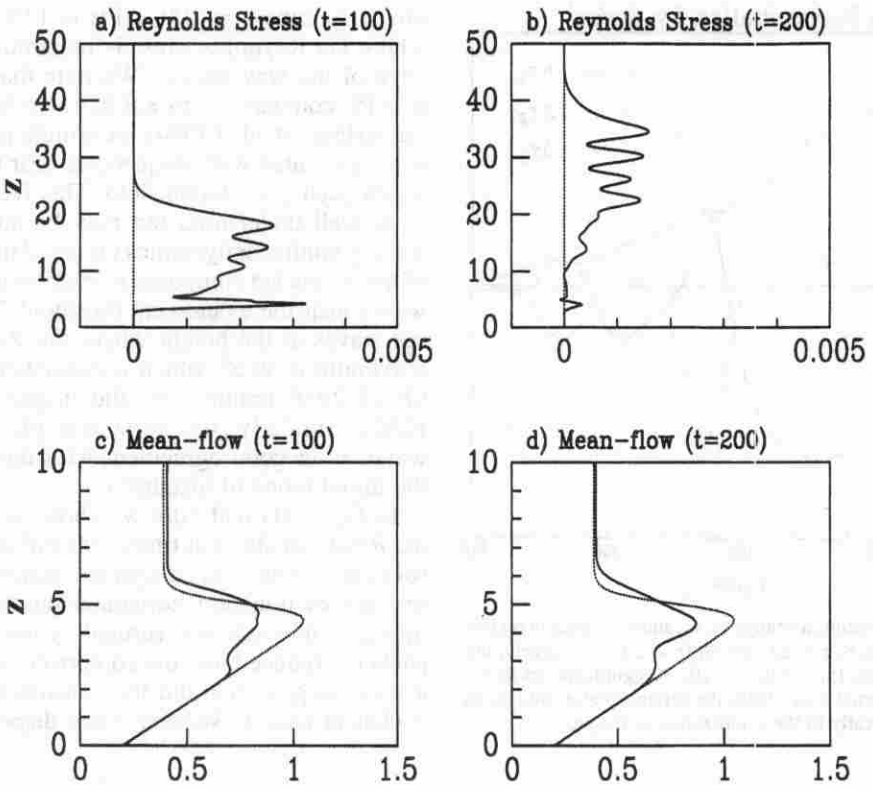

FIG. 6. Reynolds stress profiles for case 1 at times (a) $t = 100$ and (b) 200. An upward vertical flux of horizontal momentum is associated with the wavepacket at both times. The wavepacket moves upward and the vertical extent broadens primarily due to wave dispersion. Mean-flow profiles (solid curves) at times (c) $t = 100$ and (d) $t = 200$ are compared with the initial mean flow (dashed curves) in the region below $z = z_c$. The loss of momentum, most significantly near the lower critical layer, from the jet is accounted for by wave momentum transport.

with $U(z)$ defined by parameters $z_0 = 5.0$ and $R_0 = 0.3$. In this case the shear on the upper flank of the jet is initially stronger than in case 1, so the minimum gradient Richardson number is smaller, as shown explicitly in Fig. 8b. Because the speed of the jet at the upper inflection point varies little from case 1 to case 2, the effect of reducing the depth of the shear layer, which determines the spatial characteristics of the most unstable mode, is to increase the frequency of the mode. Therefore, the phase tilt of IGWs that are excited in the upper region by this instability must be such that the waves are more vertically oriented than those excited in case 1, even though the growth rate of the instability is increased. This result does not contradict the observation by McIntyre and Weissman (1978) that the penetration depth into the far field of a normal mode should be smaller for a mode of faster growth rate since the waves in case 2 do decrease in amplitude with height at a greater rate than the waves in case 1. These expectations may be verified by determining the characteristics of the most unstable mode that are delivered by a linear stability analysis. These characteristics are listed in Table 2. The perturbation streamfunction amplitude of the most unstable mode, which is shown in Fig. 8c, undulates in the region above the jet, though the vertical wavelength is longer in this case. Nonetheless, the absolute value of the penetration ratio exceeds 1, so IGWs are expected to be excited during the development of the instability. Even though Θ_Ω is smaller, the vertical group velocity is almost as large as in case 1. The waves are therefore expected to penetrate almost as deeply into the model stratosphere over the same time period.

The results of the numerical simulation are depicted for times 100 and 200 in Fig. 9. Qualitatively, these results are similar to those shown in Fig. 5 for case 1: waves are continuously excited by the large-scale structures in the mixing region until the flow stabilizes: the wavepacket propagates upward at a comparable but somewhat reduced speed; the low-level flow is nearly parallel at $t = 200$. Indeed, in case 2 the mean flow is Richardson number stable for $t > 227$, after which time the low-level flow has returned to a predominantly parallel form.

The waves emitted in case 2 are again compared quantitatively with the properties of plane IGWs in Ta-

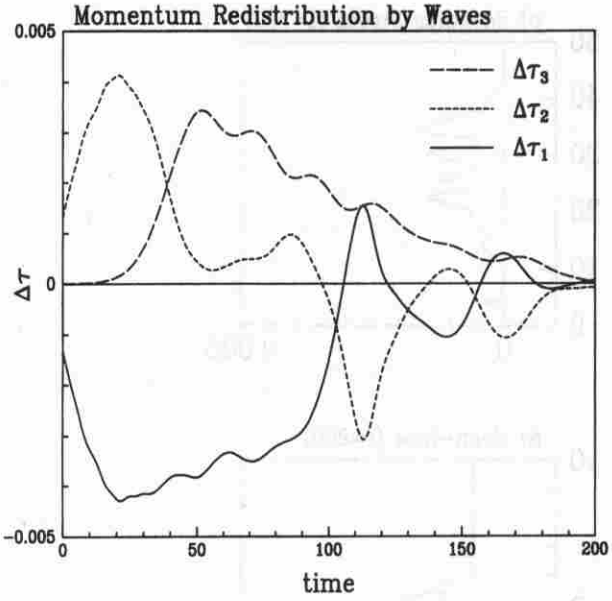

FIG. 7. The total momentum change τ_1, τ_2, and τ_3 vs time in regions $\mathcal{R}_1$ ($0 \leq z \leq z_0$), $\mathcal{R}_2$ ($z_0 \leq z \leq z_t$), and $\mathcal{R}_3$ ($z \geq z_t$), respectively, due to wave momentum flux ($z_0 = 5.0$, $z_t = 10$). A significant amount of momentum is transported away from the mixing region into $\mathcal{R}_3$ by waves contributing greatly to the stabilization of the jet.

ble 3. At time $t = 100$, APE is 13% larger than KE where the Reynolds stress is maximum at the leading edge of the wavepacket. We note that a small excess of APE compared with KE has also been observed by Sutherland et al. (1994) in simulations where IGW were generated with frequencies near the Brunt–Väisälä frequency in the far field. This feature is not presently well understood but may be attributable to the weakly nonlinear dynamics involved in the propagation of a wavepacket composed primarily of high-frequency waves near the evanescent threshold. The phase tilt of the waves at the height where the Reynolds stress is maximum is 30.5°, which is consistent with the phase tilt of 29.9° required by the dispersion relation for IGWs. Similarly, the horizontal phase speed of the waves is in good agreement with the phase speed of the initial mode of instability.

In Figs. 10a and 10b, we show vertical profiles of the Reynolds stress at times 100 and 200, respectively, for case 2. Again this diagnostic analysis demonstrates that waves transport horizontal momentum vertically upward, although the vertical group velocity of the packet is reduced and the composite waves disperse to a lesser degree than did the constituents of the wavepacket in case 1. Weaker wave dispersion is entirely

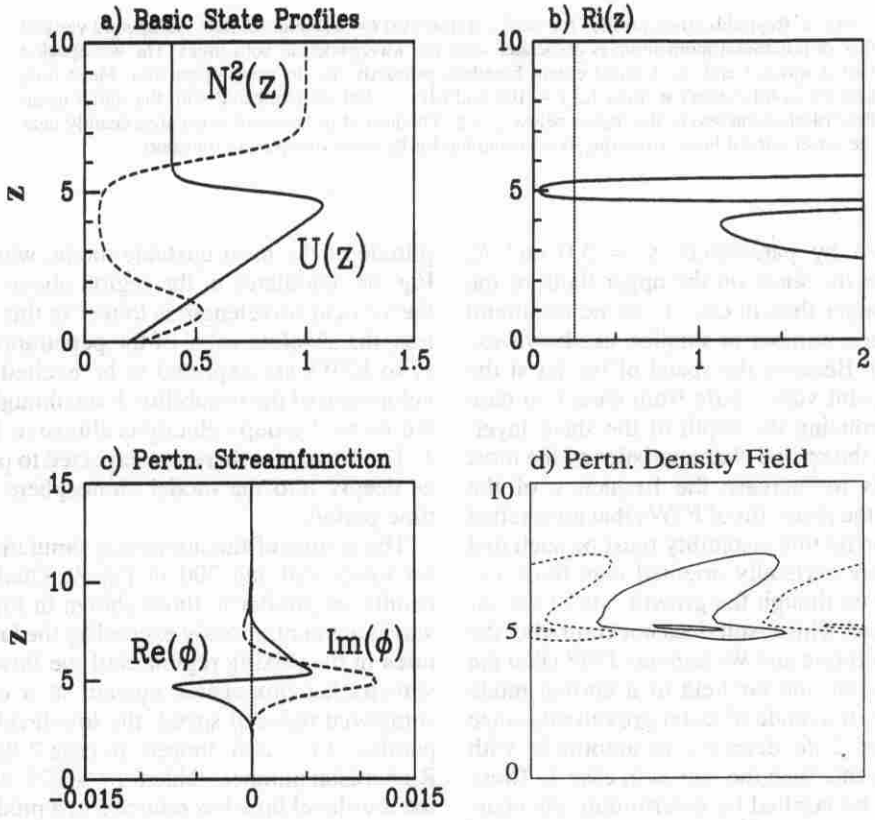

FIG. 8. Initial state as in Fig. 4 but for case 2. Contour interval in (d) is 0.01. In this case the most unstable mode couples directly with the IGW field, but the phase tilt of the waves in the upper region is more vertical.

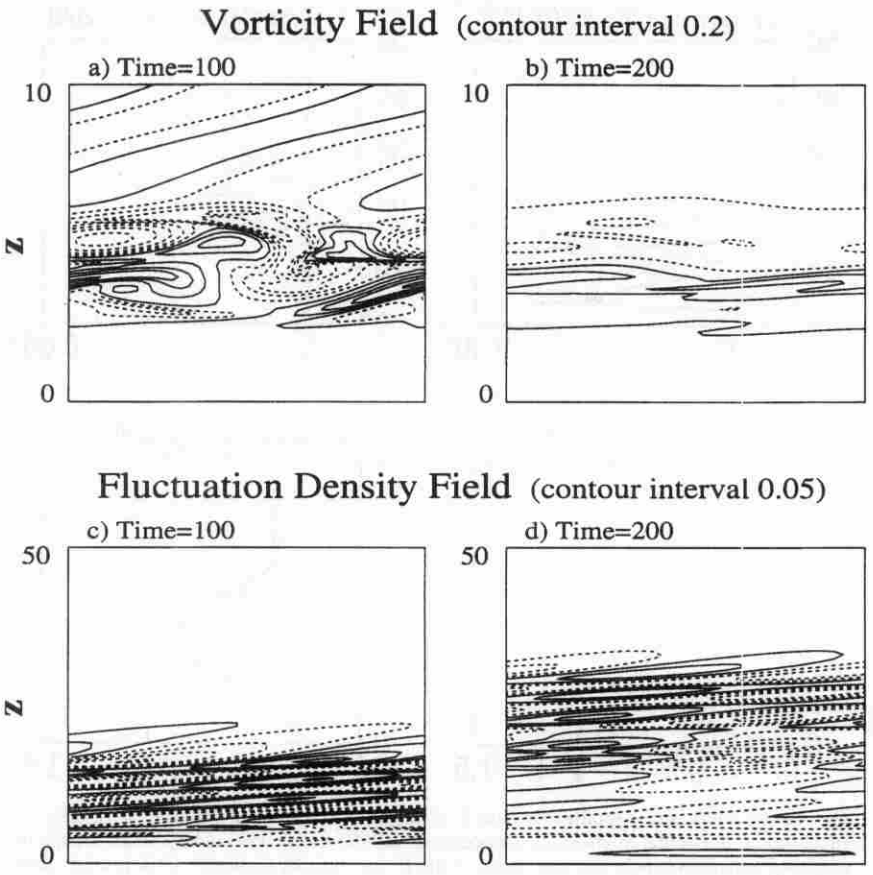

FIG. 9. From the simulation for case 2, contours of vorticity at times (a) $t = 100$ and (b) 200 and contours of perturbation density at times (c) $t = 100$ and (d) 200. Waves are excited by the large-scale features of the flow as in case 1. The wavepacket propagates upward in time with slower group velocity and with vertically steeper downstream phase tilt. The jet eventually evolves to a stable parallel flow.

expected in this case, since the intrinsic frequency of the most unstable mode in the far field is close to the Brunt–Väisälä frequency, and disturbances of marginally higher frequency are evanescent. Because dispersion is weak at the leading edge of the wavepacket, the speed with which the region of peak Reynolds stress at the leading edge of the wavepacket moves upward is an adequate measure of the vertical group velocity. The average upward speed of propagation of this feature, calculated between $t = 100$ and 200, is 0.139 (7.0 m s^{-1}), which equals the vertical group velocity of IGWs predicted by the linear stability analysis. The maximum Reynolds stress at $z = z_t$ is 0.0054 (1.46 N m^{-2}), which occurs at $t = 54$ (30 min) of nondimensional model time. This value is even larger than the maximum momentum flux recorded at this level in case 1. That the loss of momentum from the jet due to vertical wave momentum transport by IGWs is large is illustrated qualitatively in Figs. 10c and 10d, which shows the mean flow at times $t = 100$ and 200, respectively, compared with the mean flow in the basic state (dashed curve). As in case 1, the jet in case 2 is greatly decelerated near the lower critical layer. Likewise, wave radiation should contribute greatly to the stabilization process of the mean flow. Indeed, the stabilization ratio is $\mathcal{S} \approx 0.70$, indicating that the transport by IGWs of momentum from the mean flow at low levels enhances the stabilization of the mean flow to approximately the same degree as in case 1. The total momentum change as a function of time between regions $\mathcal{R}_1$, $\mathcal{R}_2$, and $\mathcal{R}_3$ is shown in Fig. 11 and compares well qualitatively with the results of case 1, although the fluctuations are more intense.

Finally in case 3 we examine circumstances for which the initial basic state N^2 profile is the same as the previous cases and $U(z)$ is defined by parameters $z_0 = 5.0$, $R_0 = 0.2$. Even though, as shown in Fig. 12b, the minimum gradient Richardson number in this case is close to zero, the shear-layer depth is so small that the frequency of the most unstable mode now exceeds the Brunt–Väisälä frequency in the model stratosphere. The instability cannot therefore couple directly into a

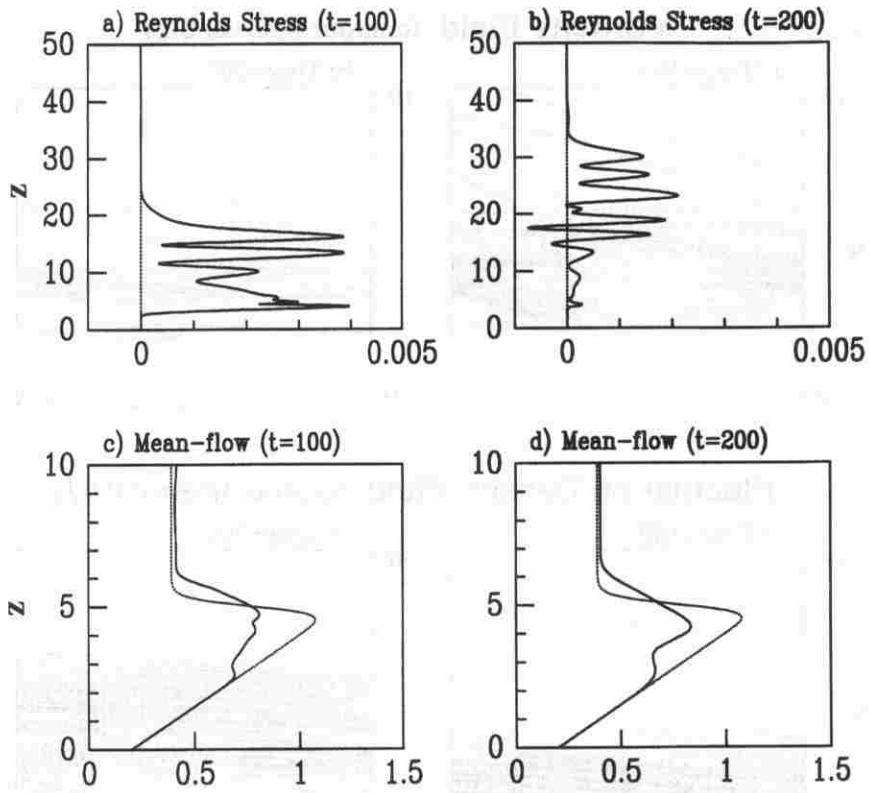

FIG. 10. Reynolds stress profiles for case 2 at times (a) $t = 100$ and (b) 200. As in case 1, a vertical flux of horizontal momentum is associated with the wavepacket at both times though the wavepacket broadens less in this case because the Brunt–Väisälä frequency limit restricts wave dispersion. Mean-flow profiles (solid curves) at times (c) $t = 100$ and (d) $t = 200$ are compared with the initial mean flow (dashed curves) in the region below $z = z_t$. The loss of momentum from this region is accounted for by wave momentum transport.

wave field in the upper region without some nonlinear enhancement. The characteristics of the most unstable mode in this case are again provided in Table 2, which shows, in particular, that the penetration condition is not satisfied in these circumstances since $|\mathcal{D}| = 0.45 < 1$. Explicitly, Fig. 12c demonstrates the evanescent nature of the fastest-growing mode of linear theory in terms of the perturbation streamfunction amplitude, and the perturbation density field presented in Fig. 12d reveals no phase tilt of the disturbance in the upper region.

Somewhat surprisingly, in our nonlinear simulations a low-amplitude wavepacket of small vertical extent propagates vertically from the level of initial instability as shown at times 100 and 200 in Fig. 13. The downstream phase tilt of the waves indicates that the disturbance propagates with positive horizontal phase speed with respect to the background flow. Unlike the previous cases we have examined, however, a single vortex centered vertically about $z = z_0$ develops nonlinearly from the most unstable mode and this vortex persists, weakening in time by interaction with the mean flow and by viscous diffusion. An analysis of the upper-level disturbance at $t = 100$ demonstrates that it is composed of IGWs since, as shown in Table 3, the APE to KE ratio is again close to unity where the Reynolds stress is largest at the leading edge of the wavepacket. At time $t = 200$ the energy ratio similarly calculated at this altitude is 1.02. On the other hand, at this level the phase tilt of the emitted waves is at an angle of 32.2° with the vertical, corresponding to a horizontal phase speed of $c_p^{(\theta)} \approx 0.68$, which is significantly less than 0.76, the phase speed of the most unstable mode of linear theory. For the frequency to be sufficiently small that the upward propagating disturbance is nonevanescent, a deceleration of the horizontal phase speed from the speed of the initial instability is required. The development of this upward propagating disturbance must therefore involve a nonlinear mechanism. This mechanism is not fully understood at present, although it would seem to be related to a deceleration of the horizontal speed of propagation of the vortex as it develops nonlinearly from the initial normal mode instability. In Sutherland et al. (1994) we have previously referred to IGW emission of this kind as involving a "secondary" generation process.

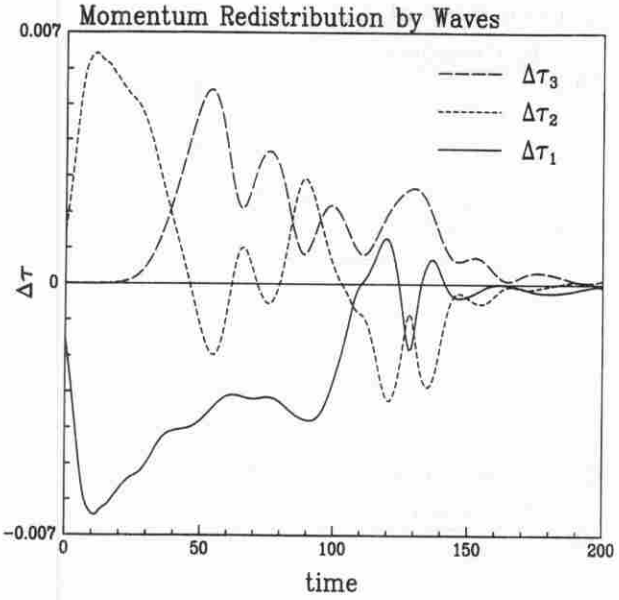

FIG. 11. The total momentum change τ_1, τ_2, and τ_3 vs time in regions $\mathcal{R}_1$ ($0 \leq z \leq z_0$), $\mathcal{R}_2$ ($z_0 \leq z \leq z_t$), and $\mathcal{R}_3$ ($z \geq z_t$), respectively, due to wave momentum flux ($z_0 = 5.0$, $z_t = 10$). A significant amount of momentum is transported away from the mixing region into $\mathcal{R}_3$ by waves contributing greatly to the stabilization of the jet.

Because there is no direct linear coupling between the excitation of waves and the growth of the instability in case 3, there are two significant consequences insofar as mean-flow evolution is concerned: far less momentum is transported into the upper region by waves, and the evolution of the flow in the long time limit is not toward a stable parallel flow but rather one in which a vortex with the same horizontal extent as the most unstable mode remains embedded in the mean flow. The flow is unstable, in the sense that $\mathrm{Ri}(z) < 1/4$ for some z, for much longer times in case 3. Though the Reynolds stress profiles of the flow at $t = 100$ and 200 shown in Figs. 14a and 14b, respectively, indicate that the wavepacket transports momentum upward, the flux is over an order of magnitude smaller than that recorded in cases 1 and 2. Similarly, Table 3 shows that the peak Reynolds stress at $z = z_t$ is much less than the peak Reynolds stress observed in the previous two cases. The effect of the nonlinear wave excitation mechanism on the development and stabilization of the mean flow appears to be negligible since, as the mean-flow profiles in Figs. 14c and 14d indicate, the local redistribution of momentum about z_0 is largely responsible for the gradual weakening of the strength of the shear. There is also negligible loss of momentum near the lower

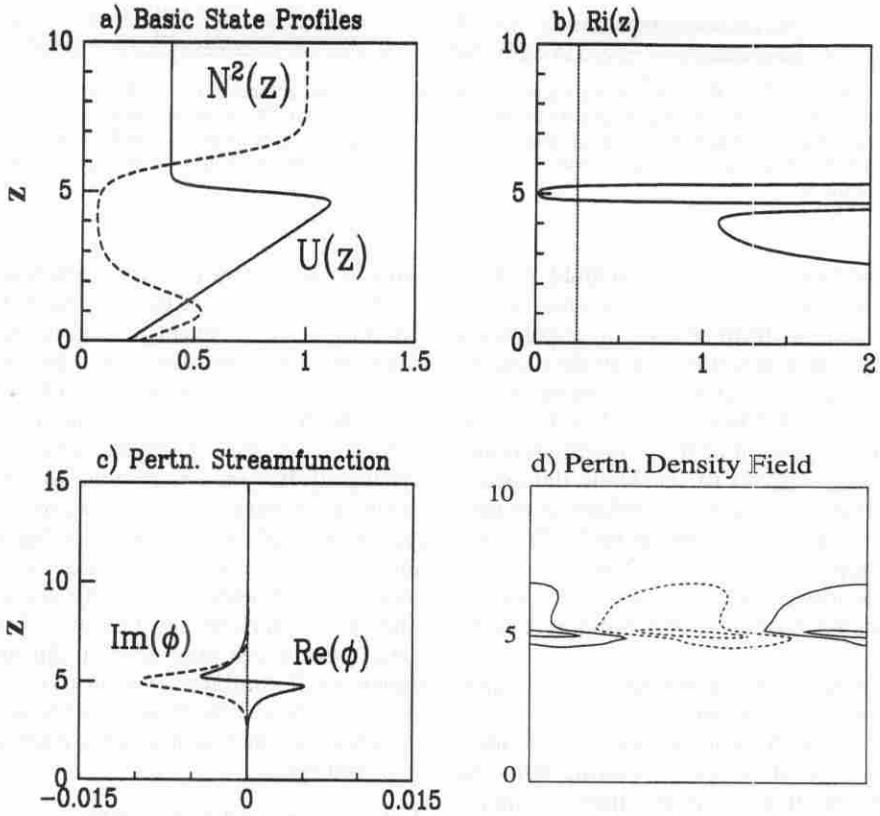

FIG. 12. Initial state as in Fig. 4 but for case 3. Contour interval in (d) is 0.005. In this case the most unstable mode does not couple with a propagating wave field since the frequency of the normal mode exceeds the Brunt–Väisälä frequency.

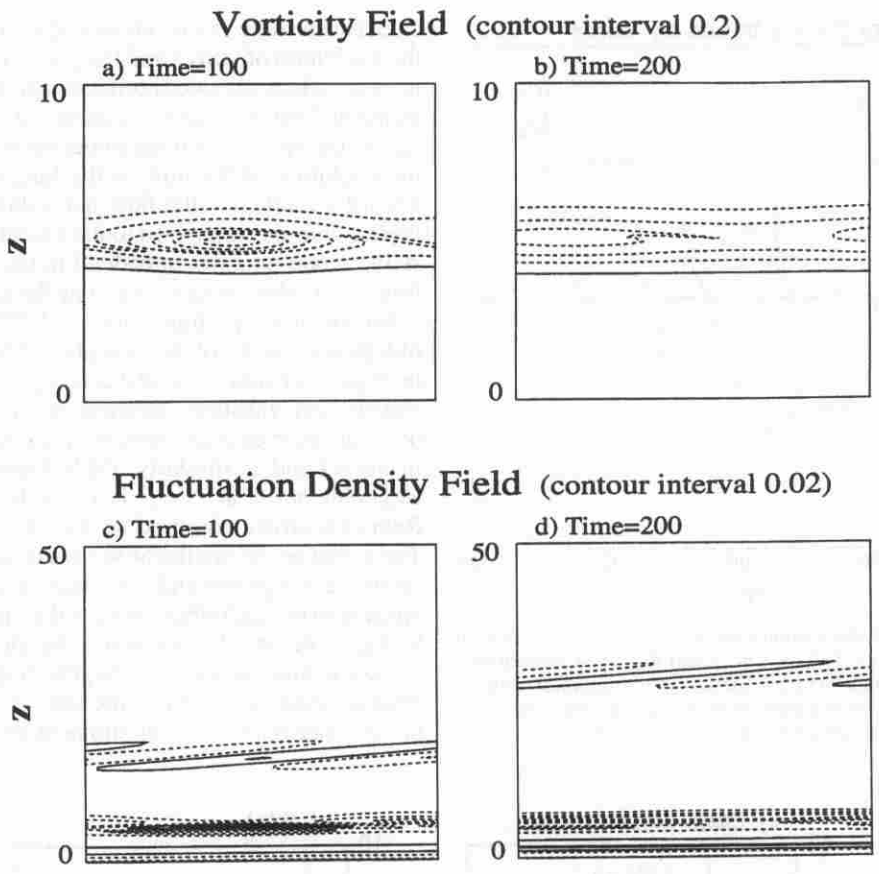

FIG. 13. From the simulation for case 3, contours of vorticity at times (a) $t = 100$ and (b) 200 and contours of perturbation density at times (c) $t = 100$ and (d) 200. A small-amplitude wavepacket propagates upward in time. These waves are excited through a nonlinear mechanism. The simulation evolves to a state in which a vortex is embedded in the mean flow on the upper flank of the jet.

critical layer. Similarly, after a comparably small change in momentum in $\mathcal{R}_3$, Fig. 15 shows a monotonic extraction of momentum from $\mathcal{R}_1$ into $\mathcal{R}_2$ superposed with small periodic variations attributed to the nutation of the core of the residual vortex. These observations are quantified by the stabilization ratio $\mathcal{S} \approx 0.11$, indicating that about 90 percent of the momentum transported by waves across z_0 act to accelerate the jet directly above z_0. This final vortex-embedded state persists because momentum is not transported efficiently from the mixing region by waves, and so the energy associated with the wave of the same horizontal extent as the most unstable normal mode remains locally trapped.

In simulations of case 3 in a larger horizontal domain that allows the growth of more than one wavelength of the most unstable mode, a richer variety of outcomes is permissible. In general, however, pairing between vortices is greatly inhibited by the proximity of the region of enhanced static stability near z_0 so that the mean flow becomes stable and the vortices weaken due to viscous diffusion before pairing events occur. The same is true of simulations performed with Re = 4000. Should vortex merger occur in higher Reynolds number flow, such an event may give rise to IGWs excitation in a manner described by Davis and Peltier (1979). Even in simulations with Re = 2000 and 4000, however, asymmetric weak interactions between the vortices have been observed to excite vertically propagating IGWs superharmonic to the initial normal mode disturbance. A wave–wave interaction of this type was noted previously by Sutherland et al. (1994) and constitutes a novel nonlinear mechanism for IGW generation. Another possibility not investigated here [but see Sutherland and Peltier (1994)] is that spanwise disturbances may develop during the fully three-dimensional nonlinear evolution of the vortex-embedded mean flow. This may result in the rapid transition to turbulence and significantly more rapid mean-flow stabilization.

4. Discussion and conclusions

We have investigated a mechanism through which large amplitude IGWs may be generated by shear in-

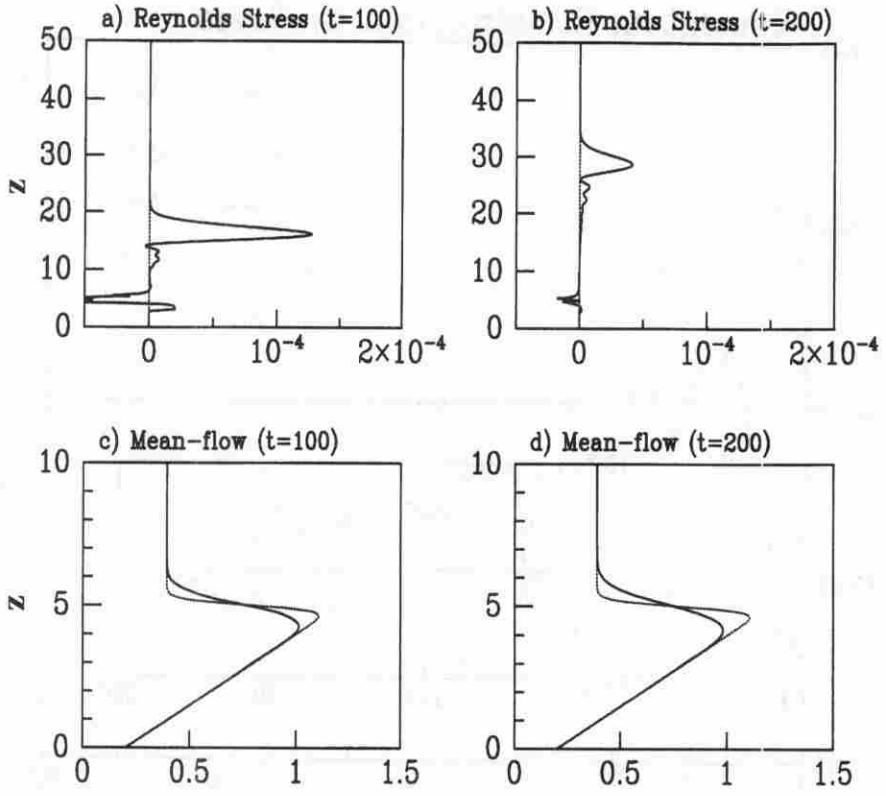

FIG. 14. Reynolds stress profiles for case 3 at times (a) $t = 100$ and (b) 200. A weak vertical flux of horizontal momentum is associated with the wavepacket at both times. Mean-flow profiles (solid curves) at times (c) $t = 100$ and (d) $t = 200$ compared with the initial mean flow (dashed curves) show that horizontal momentum is redistributed about the inflection point on the top flank of the jet and that very little momentum is extracted from the jet region.

stability in the midlatitude tropospheric jet streams of earth's atmosphere. The precondition necessary for the onset of this instability is that the maximum shear on the upper flank of the jet, which typically is situated near the tropopause, is shifted vertically downward by about 1 km into a region in which N^2 is small. Such conditions may possibly develop during a baroclinic wave lifecycle as a consequence of ageostrophic effects. The basic-state flows we have considered were motivated by observations reported by Lilly and Zipser (1972) of the lower atmosphere upstream of a downslope windstorm induced by the breaking of topographically forced internal waves (Peltier and Clark 1979). We constructed an analytic approximation to the observed $N^2(z)$ profile and an analytic expression for the zonal velocity profile $U(z)$ that is characterized by two parameters representing the altitude z_0 of the point of maximum vertical shear on the upper flank of the jet stream and the shear layer half-depth R_0. In a sequence of two-dimensional nonlinear simulations we considered three cases, in all of which $z_0 = 5.0$ and $R_0 = 0.4$ (case 1), $R_0 = 0.3$ (case 2), and $R_0 = 0.2$ (case 3). In all three cases the gradient Richardson number was initially less than 1/4 only over a vertical range including the upper flank of the jet stream. In all three cases linear stability analysis confirmed the initial flow to be unstable to normal mode disturbances.

In cases 1 and 2, the most unstable mode couples directly (i.e., linearly) with IGWs in the region above the jet stream and continuous wave emission into the middle atmosphere occurs until the mean flow is stabilized. (That is, the vertical profile of the gradient Richardson number of the horizontally averaged flow exceeds 1/4 everywhere). Diagnostic analyses of these simulated flows were shown to provide convincing evidence that the IGWs are indeed excited directly by the most unstable mode of linear stability theory: the phase tilt of the waves is the same as that predicted by linear theory on the basis of the dispersion relation, and the horizontal phase speed and wavelength of the waves are the same as those of the most unstable mode. Characteristic of plane IGWs, in case 1 the energy of the wavepacket is equally partitioned between APE and KE. In case 2, however, APE is 13 percent larger than KE. We expect that this characteristic of the emitted wavepacket arises as a consequence of weakly nonlinear processes coupled with the influence of dispersion of the constituent waves of the packet that consists pri-

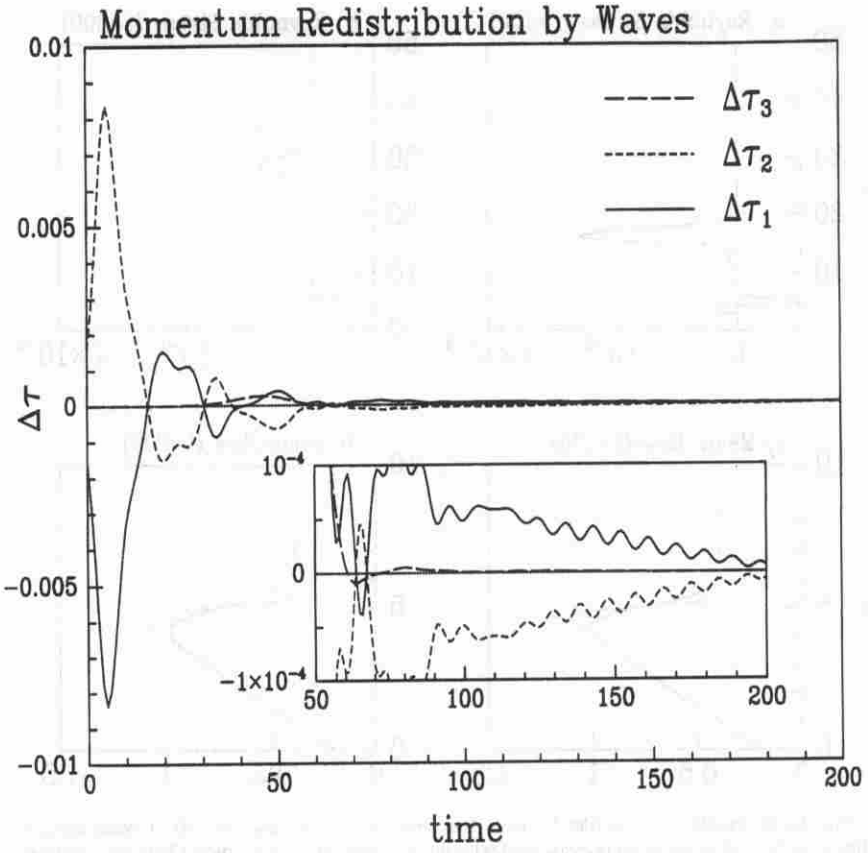

FIG. 15. The total momentum change τ_1, τ_2, and τ_3 vs time in regions $\mathcal{R}_1$ ($0 \leq z \leq z_0$), $\mathcal{R}_2$ ($z_0 \leq z \leq z_t$), and $\mathcal{R}_3$ ($z \geq z_t$), respectively, due to wave momentum flux ($z_0 = 5.0$, $z_t = 10$). The inset shows the same curves on a finer scale between times 50 and 200. Momentum is transported across $z = z_0$ as the vortex nutates, but very little momentum is transported away from the mixing region into $\mathcal{R}_3$ by waves.

marily of waves whose frequencies are near the Brunt–Väisälä frequency. In both cases, the Reynolds stress recorded directly above the jet is as large as that occurring over topography during the strongest observed downslope windstorm events (Palmer et al. 1986). Indeed, the excitation of IGWs is shown to greatly contribute to the stabilization of the flow by way of transporting zonal momentum vertically away from the jet stream into the lower stratosphere; the mixing region on the upper flank of the jet stream thereafter evolves toward a state of stable parallel flow. Although fully three-dimensional nonlinear simulations of the wave generation process have yet to be performed, the fact that these IGWs are coupled directly to the growth of the most unstable mode of linear stability theory requires, on the basis of Squire's theorem (Squire 1933), that the initial stages of flow evolution be two-dimensional, and we therefore expect that the addition of a third degree of freedom to the simulations will not affect the IGW emission that occurs during the early stages of the nonlinear evolution of the flow.

In case 3, the initial shear depth on the top flank of the jet was fixed to be so small that the frequency of the most unstable mode was greater than the Brunt–Väisälä frequency in the overlying stratosphere. As a result, the most unstable mode does not couple with a nonevanescent wave field in the region above the jet, and thus propagating IGWs are not excited by the linear growth of the mode. Nonetheless, a low-amplitude vertically confined IGW wavepacket does propagate upward in the simulation. Examination shows that the horizontal phase speed of the waves is smaller than that of the most unstable mode so that a nonlinear mechanism is responsible for the generation of the wavepacket. For this reason, very little momentum is transported vertically away from the jet, and the long time evolution of the flow is dominated by a vortex–mean flow interaction. It is reasonable to assume, however, that in a three-dimensional analysis spanwise perturbations and fully developed turbulence would contribute strongly in this case to rapid stabilization of the flow.

We have chosen to present here the analyses of the nonlinear simulations of cases 1, 2, and 3 in detail because they demonstrate a critical regime of the parameter space (R, z_0) for which the linear mechanism for the excitation of IGWs is switched off, as in case 3, for

sufficiently small values of the shear depth R. To demonstrate the robustness of the linear excitation mechanism, we have performed a linear stability analysis for inviscid fluid of a series of tropospheric jet flows. In this study we consider the original $U(z)$ and $N^2(z)$ profiles obtained from Lilly and Zipser (1972) and, without adjusting $U(z)$ below the jet maximum, we examine the effect of two adjustments to the shear on the upper flank of the jet alone: shifting the altitude of the region of maximum shear downward by an amount z_s and decreasing the depth of the shear by a scaling factor D. To this end, the perturbed mean flow is given by

$$U(z; D, z_s) = \begin{cases} U\left(\dfrac{(z - z_0)}{D + z_0 - z_s}\right), & \dfrac{(z - z_0)}{D + z_0 - z_s} \geqslant z_m \\ U(z - z_s), & z - z_s \leqslant z_m, \end{cases} \quad (22)$$

where z_m is the altitude of the jet maximum. A cubic spline is used to define $U(z; D, z_s)$ for $z_m + z_s < z < z_0 + D(z_m - z_0 + z_s)$. The stability regimes of the parameter space shown in Fig. 16 demonstrate that the penetration condition is satisfied by the most unstable mode in flows for a wide range of parameters D and z_s provided that $z_s > 1$ km. If both D and z_s are large, then the penetration condition may not be satisfied by the most unstable mode but the frequency of the mode may be less than the Brunt–Väisälä frequency and so the phase speed condition, which was first proposed by McIntyre and Weissman (1978), is satisfied. Under these circumstances strong radiation may occur but, because $|\mathcal{D}| < 1$, nonlinear processes are expected to play a necessary role in the formation of a propagating wavepacket. The results of two-dimensional nonlinear simulations of flows for which the phase speed condition is satisfied and $|\mathcal{D}| < 1$ are not shown here but these do indeed show strong IGW excitation, though the time-integrated vertical flux of horizontal momentum away from the mixing region is generally less than it is in cases for which $|\mathcal{D}| > 1$. Whether or not the penetration condition is satisfied, the vertical momentum flux predicted from two-dimensional simulations may be overestimated from that in a fully three-dimensional flow in which turbulence may develop more rapidly and large-scale structures are strained to small scales. However, the development of turbulence would presumably pose greater restrictions to the generation of IGW generation in cases for which $|\mathcal{D}| < 1$.

The results reported herein may have important implications for the parameterization of internal gravity wave drag in atmospheric general circulation models. The horizontal wavelength of the propagating disturbances is less than 10 km in each simulation, which is well below the horizontal resolution that will be available in atmospheric GCMs in the foreseeable future. Nonetheless, because the momentum flux effected by the emitted waves can be large, as large as the fluxes observed in severe downslope windstorm events, the wave drag exerted on the middle atmosphere by breaking waves should be as important as the wave drag associated with topographic forcing and perhaps at least as ubiquitous. In parameterizing the drag due to this mechanism, however, we must take into account not only the acceleration of the flow by breaking waves in the middle atmosphere but also the deceleration of the tropospheric jet itself by the wave emission process. A reasonable accounting for this radiation reaction could prove challenging since the strong wave radiation apparent in cases 1 and 2 is inhibited in case 3 due to a relatively small decrease in the shear depth R_0 of the initial basic state. As well as being sensitive to the shear depth, we have found in simulations not shown here that the IGW excitation mechanism is also sensitive to the initial altitude z_0 of the upper inflection point of the tropospheric jet. To appropriately parameterize the effects of this mechanism, therefore, a detailed examination of the full range of preconditions that lead to either radiating or nonradiating instability should be performed. This would require better in situ measurements of horizontal velocity and potential temperature profiles during the development of fronts and synoptic-scale cyclones. Detailed simulations at higher resolutions than have previously been performed of baroclinic wave life cycles would help immeasurably, since it seems clear that published analyses

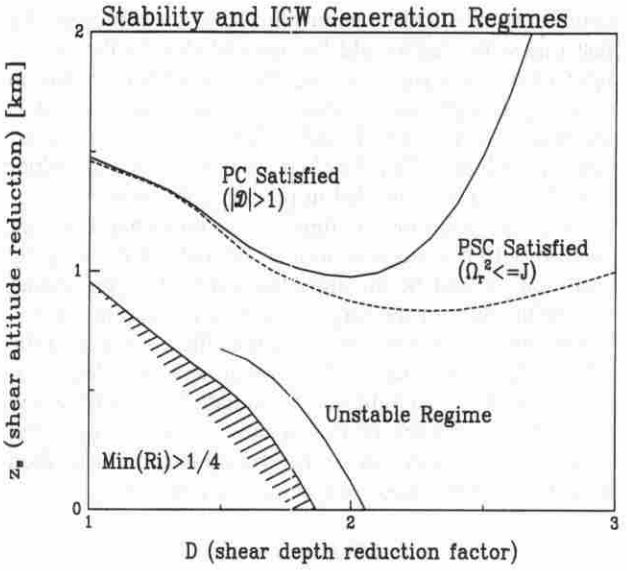

FIG. 16. The stability regimes of the perturbed tropospheric jet determined using the original N^2 profile of Lilly and Zipser (1972) and with $U(z; D, z_s)$ given by (22), in which D is the scaling factor by which the shear depth on the upper flank of the tropospheric jet is reduced and z_s is the altitude by which the inflection point of the shear is lowered; $D = 1$, and $z_s = 0$ corresponds to unperturbed flow. The region above the dashed line (where $z_s > 1$ km) denotes the regime of parameters (D, z_s) for which the Doppler-shifted frequency of the most unstable mode is less than $N(z)$ at large z. In this region the phase speed condition is satisfied. Within this region is the regime above the solid line in which the penetration condition is satisfied. The flow is stable, and the minimum gradient Richardson number exceeds 1/4 for small values of D and z_s.

could not realistically capture the IGW dynamics on the fast timescale that would be associated with the development of the instabilities we have described within an evolving synoptic-scale cyclone. In the near future it is intended that the recently published analyses of Polavarapu and Peltier (1990, 1993a,b) and of Bush and Peltier (1994, 1995) be extended in precisely this way.

One final point that is important to understand in connection with our suggestion that "gravity wave drag by emission" could be an important interaction governing the architecture of the large-scale flow, concerns the extent to which this interaction requires the existence of the "N^2 notch." It may well be that spatially localized patches of KH-instability could radiate IGWs efficiently even in the absence of this feature, in which case the process of "gravity wave drag by emission" described herein would be expected to be commonplace.

REFERENCES

Boer, G., and Coauthors, 1992: Some results from an intercomparison of the climates simulated by 14 atmospheric general circulation models. *J. Geophys. Res.*, **97**(D12), 12 771–12 786.

Bush, A., and W. Peltier, 1994: Tropopause folds and synoptic-scale baroclinic wave life cycles. *J. Atmos. Sci.*, **51,** 1581–1604.

——, J. McWilliams, and W. Peltier, 1995: The origins and evolution of "imbalance" in synoptic-scale baroclinic wave life cycles. *J. Atmos. Sci.*, **52,** 1051–1069.

Chimonas, G., and J. Grant, 1984: Shear excitation of gravity waves. Part II: Upscale scattering from Kelvin–Helmholtz waves. *J. Atmos. Sci.*, **41,** 2278–2288.

Clark, T. L., T. Hauf, and J. P. Kuettner, 1986: Convectively forced internal gravity waves: Results from two-dimensional numerical experiments. *Quart. J. Roy. Meteor. Soc.*, **112,** 899–925.

Davis, P., and W. Peltier, 1976: Resonant parallel shear instability in the stably stratified planetary boundary layer. *J. Atmos. Sci.*, **33,** 1287–1300.

——, and ——, 1979: Some characteristics of the Kelvin–Helmholtz and resonant overreflection modes of shear flow instability and of their interaction through vortex pairing. *J. Atmos. Sci.*, **36,** 2394–2412.

Fovell, R., D. Durran, and J. R. Holton, 1992: Numerical simulations of convectively generated stratospheric gravity waves. *J. Atmos. Sci.*, **49,** 1427–1442.

Fritts, D., 1982: Shear excitation of atmospheric gravity waves. *J. Atmos. Sci.*, **39,** 1936–1952.

——, 1984: Shear excitation of atmospheric gravity waves. Part II: Nonlinear radiation from a free shear layer. *J. Atmos. Sci.*, **41,** 524–537.

——, and G. Nastrom, 1992: Sources of mesoscale variability of gravity waves. Part II: Frontal, convective, and jet stream excitation. *J. Atmos. Sci.*, **49,** 111–127.

Gill, A., 1982: *Atmosphere-Ocean Dynamics.* Academic Press, 662 pp.

Herron, T., and I. Tolstoy, 1969: Tracking jet stream winds from ground level pressure signals. *J. Atmos. Sci.*, **26,** 266–269.

Hines, C., 1960: Internal atmospheric gravity waves at ionspheric heights. *Can. J. Phys.*, **38,** 1441–1481.

Hodges, R. R., Jr., 1967: Generation of turbulence in the upper atmosphere by internal gravity waves. *J. Geophys. Res.*, **72,** 3455–3458.

——, 1969: Eddy diffusion coefficients due to instabilities in internal gravity waves. *J. Geophys. Res.*, **74,** 4087–4090.

Hooke, W., Jr., F. H., and E. Gossard, 1973: Observed generation of an atmospheric gravity wave by shear instability in the mean flow of the planetary boundary layer. *Bound.-Layer Meteor.*, **5,** 29–41.

Howard, L., 1961: Note on a paper by John W. Miles. *J. Fluid Mech.*, **10,** 509–512.

Jones, W., 1968: Reflexion and stability of waves in stably stratified fluids with shear flow: A numerical study. *J. Fluid Mech.*, **34,** 609–624.

Keliher, T., 1975: The occurrence of microbarograph-detected gravity waves compared with the existence of dynamically unstable wind shear layers. *J. Geophys. Res.*, **80,** 2967–2976.

Klaassen, G., and W. R. Peltier, 1985: The onset of turbulence in finite-amplitude Kelvin–Helmholtz billows. *J. Fluid Mech.*, **155,** 1–35.

Lalas, D., and F. Einaudi, 1976: On the characteristics of gravity waves generated by atmospheric shear layers. *J. Atmos. Sci.*, **33,** 1248–1259.

Lilly, D., and E. J. Zipser, 1972: The front range windstorm of 11 January 1972—A meteorological narrative. *Weatherwise,* **25,** 56–63.

——, and P. J. Kennedy, 1973: Observations of a stationary mountain wave and its associated momentum flux and energy dissipation. *J. Atmos. Sci.*, **30,** 1135–1152.

Lindzen, R. S., 1967: Thermally driven diurnal tide in the atmosphere. *Quart. J. Roy. Meteor. Soc.*, **93,** 18–42.

——, 1974: Stability of a Helmholtz velocity profile in a continuously stratified infinite Boussinesq fluid—Applications to clear air turbulence. *J. Atmos. Sci.*, **31,** 1507–1514.

——, 1981: Turbulence and stress owing to gravity wave and tidal breakdown. *J. Geophys. Res.*, **86,** 9707–9714.

——, and A. Rosenthal, 1976: On the instability of Helmholtz velocity profiles in stably stratified fluids when a lower boundary is present. *J. Geophys. Res.*, **81**(9), 1561–1571.

——, and J. Barker, 1985: Instability and wave over-reflection in stably stratified shear flow. *J. Fluid Mech.*, **151,** 189–217.

Lott, F., H. Kelder, and H. Teitelbaum, 1992: A transition from Kelvin–Helmholtz instabilities to propagating wave instabilities. *Phys. Fluids Ser. A,* **4,** 1990–1997.

Manson, A., and Coauthors, 1991: Comparisons between satellite-derived gradient winds and radar-derived winds from the CIRA-86. *J. Atmos. Sci.*, **48,** 411–428.

Mastrantonio, G., F. Einaudi, D. Fua, and D. Lalas, 1976: Generation of gravity waves by jet streams in the atmosphere. *J. Atmos. Sci.*, **33,** 1730–1738.

McFarlane, N., 1987: The effect of orographically excited gravity wave drag on the general circulation of the lower stratosphere and troposphere. *J. Atmos. Sci.*, **44,** 1775–1800.

——, G. Boer, J.-P. Blanchet, and M. Lazare, 1992: The Canadian Climate Centre second-generation general circulation model and its equilibrium climate. *J. Climate,* **5,** 1013–1044.

McIntyre, M., and M. Weissman, 1978: On radiating instabilities and resonant overreflection. *J. Atmos. Sci.*, **35,** 1190–1196.

Miles, J., 1961: On the stability of heterogeneous shear flows. *J. Fluid Mech.*, **10,** 496–508.

Palmer, T. N., G. J. Shutts, and R. Swinbank, 1986: Alleviation of a systematic westerly bias in general circulation and numerical weather prediction models through an orographic gravity drag parameterization. *Quart. J. Roy. Meteor. Soc.*, **112,** 1001–1039.

Peltier, W., and T. Clark, 1979: The evolution and stability of finite-amplitude mountain waves. Part II: Surface wave drag and severe downslope windstorms. *J. Atmos. Sci.*, **36,** 1498–1529.

——, and ——, 1980: Reply. *J. Atmos. Sci.*, **37,** 2122–2125.

Polavarapu, S., and W. Peltier, 1990: The structure and nonlinear evolution of synoptic scale cyclones: Life cycle simulations with a cloud-scale model. *J. Atmos. Sci.*, **47,** 2645–2672.

——, and ——, 1993a: Formation of small-scale cyclones in numerical simulations of synoptic-scale baroclinic wave life cycles: Secondary instability at the cusp. *J. Atmos. Sci.*, **50,** 1047–1057.

——, and ——, 1993b: The structure and nonlinear evolution of synoptic-scale cyclones. Part II: Wave–mean flow interaction and asymptotic equilibration. *J. Atmos. Sci.*, **50,** 3164–3184.

Smyth, W., and W. Peltier, 1989: The transition between Kelvin–Helmholtz and Holmboe instability: An investigation of the overreflection hypothesis. *J. Atmos. Sci.*, **46,** 3698–3720.

Squire, H., 1933: On the stability of three-dimensional disturbances of viscous flow between parallel walls. *Proc. Roy. Soc. Ser. A,* **142,** 621–628.

Sutherland, B., and W. Peltier, 1992: The stability of stratified jets. *Geophys. Astrophys. Fluid Dyn.*, **66,** 101–131.

——, and ——, 1994: Turbulence transition and internal wave generation in density stratified jets. *Phys. Fluids Ser. A,* **6,** 1267–1284.

——, C. Caulfield, and W. Peltier, 1994: Internal wave generation and hydrodynamic instability. *J. Atmos. Sci.*, **51,** 3261–3280.